MEMORANDUM REPORT BRL-MR-3687

(SUPERSEDES IMR-0896)

BRL

1938 – Serving the Army for Fifty Years – 1988

AERODYNAMICS ANALYSIS OF SOLID FUEL RAMJET PROJECTILES

ASHER SIGAL
JAMES E. DANBERG

MAY 1988

U.S. ARMY LABORATORY COMMAND

BALLISTIC RESEARCH LABORATORY

ABERDEEN PROVING GROUND, MARYLAND

UNCLASSIFIED
SECURITY CLASSIFICATION OF THIS PAGE

REPORT DOCUMENTATION PAGE

Form Approved OMB No. 0704-0188

1a. REPORT SECURITY CLASSIFICATION UNCLASSIFIED	1b. RESTRICTIVE MARKINGS
2a. SECURITY CLASSIFICATION AUTHORITY	3. DISTRIBUTION/AVAILABILITY OF REPORT Approved for public release, distribution unlimited.
2b. DECLASSIFICATION/DOWNGRADING SCHEDULE	
4. PERFORMING ORGANIZATION REPORT NUMBER(S) BRL-MR-3687	5. MONITORING ORGANIZATION REPORT NUMBER(S)
6a. NAME OF PERFORMING ORGANIZATION U.S. Army Ballistic Research Laboratory 6b. OFFICE SYMBOL (If applicable) SLCBR-LF	7a. NAME OF MONITORING ORGANIZATION
6c. ADDRESS (City, State, and ZIP Code) Aberdeen Proving Ground, Maryland 21005-5066	7b. ADDRESS (City, State, and ZIP Code)
8a. NAME OF FUNDING/SPONSORING ORGANIZATION 8b. OFFICE SYMBOL (If applicable)	9. PROCUREMENT INSTRUMENT IDENTIFICATION NUMBER
8c. ADDRESS (City, State, and ZIP Code)	10. SOURCE OF FUNDING NUMBERS PROGRAM ELEMENT NO. / PROJECT NO. / TASK NO. / WORK UNIT ACCESSION NO.

11. TITLE (Include Security Classification)

AERODYNAMIC ANALYSIS OF SOLID FUEL RAMJET PROJECTILES

12. PERSONAL AUTHOR(S)

SIGAL, ASHER (NRC) and DANBERG, JAMES E.

13a. TYPE OF REPORT	13b. TIME COVERED	14. DATE OF REPORT (Year, Month, Day)	15. PAGE COUNT
Memorandum Report	FROM _____ TO _____		

16. SUPPLEMENTARY NOTATION

17. COSATI CODES			18. SUBJECT TERMS (Continue on reverse if necessary and identify by block number)		
FIELD	GROUP	SUB-GROUP	SFRJ Projectile	60mm SFRJ-FINNER	Inlet
01	19		Static Stability	40mm SFRJ	
01	01		Buttress Threads	75mm SFRJ	

19. ABSTRACT (Continue on reverse if necessary and identify by block number)

The aerodynamic characteristics of several Solid Fuel Ramjet (SFRJ) projectiles are estimated by a combination of the NSWC-Aeroprediction code and a post-processing analysis that account for the effects of inlet and the buttress threads.

Comparison between predicted and measured normal-force curve slope for two SFRJ-SPINNER configurations show good agreement in one case and 18%-23% analytical under-prediction in the other. The agreement in center-of-pressure location is very good in both cases.

The analysis explains the unstable flight of the 60mm SFRJ-FINNER Projectile, having original fins. The analysis predicts, for the projectile with extended fins, a static margin of 0.5 calibers at low supersonic Mach numbers, marginal stability as Mach number approaches 4.3 and instability at Mach numbers larger than 4.3. Wind-tunnel tests of this configuration

(continued on the reverse side)

20. DISTRIBUTION/AVAILABILITY OF ABSTRACT	21. ABSTRACT SECURITY CLASSIFICATION
☑ UNCLASSIFIED/UNLIMITED ☐ SAME AS RPT. ☐ DTIC USERS	UNCLASSIFIED

22a. NAME OF RESPONSIBLE INDIVIDUAL	22b. TELEPHONE (Include Area Code)	22c. OFFICE SYMBOL
Asher Sigal (NRC)	(301) 278-3707	SLCBR-LF-C

DD Form 1473, JUN 86 *Previous editions are obsolete.*

SECURITY CLASSIFICATION OF THIS PAGE

UNCLASSIFIED

19. ABSTRACT (Continued)

show that the open inlet contributes more normal-force than accounted for in the analysis and that contribution of the fin set is slightly underpredicted by the NSWC code. The predicted normal-force curve slope is up to 11% smaller than experimentally obtained and the center-of-pressure location is in good agreement with test results. The experimentally obtained contribution of the buttress threads to the axial-force coefficient is in good agreement with the predicted value. No effect of the threads on the stability of the projectile was observed under the wind-tunnel flow conditions.

ACKNOWLEDGMENT

Dr. R.J. Yalamanchili of the Launch and Flight Division, Mr. R. Wood of NASA Langley Research Center and Mr. D.N. Olsen and Mr. F. Wrede of the US Army Chemical Research, Development and Engineering Center, planned and carried out the wind-tunnel tests. They are thanked for making available their results for this study.

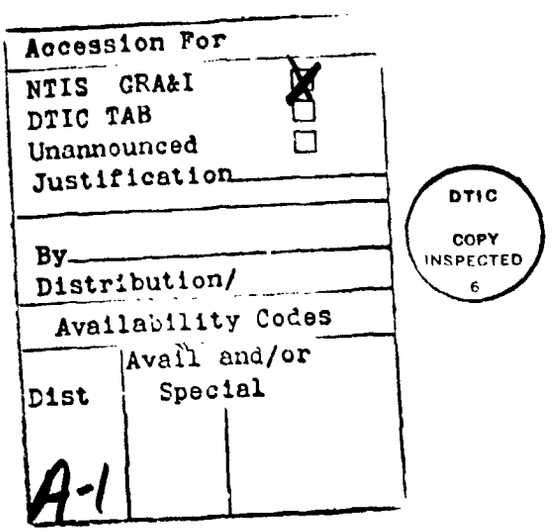

TABLE OF CONTENTS

TABLE OF CONTENTS (Continued)

LIST OF FIGURES

LIST OF FIGURES (Continued)

LIST OF FIGURES (Continued)

I. INTRODUCTION

The Solid Fuel Ramjet (SFRJ) family of projectiles is a new technology in the field of ballistics that features a capability to modulate the acceleration in flight. At present, SFRJ training rounds are being developed that simulate low drag at the initial phase of the flight and produce high deceleration past the burning time. The SFRJ family of projectiles consists of spin-stabilized and fin-stabilized configurations. Both types have Pitot type inlets. The fin-stabilized configurations have circumferential ridges or grooves that transfer the launch accelerating force.

The Missile DATCOM[1] and the NSWC Aeroprediction[2] codes, that are available at BRL, are capable of analyzing the aerodynamic characteristics of body alone and fin-body combinations. However, neither code includes an option of an inlet in the body or takes into account the aerodynamic effects associated with the roughness elements. Since the codes possess quick response capability, a hybrid scheme of analysis is devised. The available codes are used for basic analysis of model configurations. Then, corrections for the two effects that were mentioned above, are applied.

Selection of an appropriate prediction code is considered first. Then, the additional analysis is described. Finally, the application of the proposed scheme to the various SFRJ configurations is presented. The predictions are compared with available test data from wind-tunnels and ballistic ranges.

II. SELECTION OF A DESIGN CODE

The Missile DATCOM and the NSWC-Aeroprediction codes are capable of estimating the external axial force, the normal-force and the static stability of the pertinent configurations. For the analysis of body alone, in the supersonic domain, both codes offer the same analytical options: Van Dyke's[3] hybrid theory and the second order shock expansion[4] method (SOSE). Indeed, the two codes give practically the same answers when applied to the same body configuration. Only the SOSE can cover the whole supersonic Mach number range. Comparison of prediction by this method to empirical data bases showed very good agreement in normal-force curve slope and center-of-pressure. They will be discussed in Chapter IV, with regard to actual configurations.

Both codes use the supersonic lifting surface method, when applicable, for the fin alone aerodynamic characteristics.

The main difference between the codes, for the present application, is in the body-fin and fin-body influence coefficient. For fins mounted entirely on a body, both codes use Nielsen's[5] influence coefficients. For fins that over-hang the base of the body, as in the case of the 60mm

SFRJ-FINNER projectile that will be described in Chapter IV, Section 3, the DATCOM code uses the same influence coefficients. Only the NSWC code applies a correction, based on empirical data, to account for the reduction in interference normal-force associated with the over-hang. As will be elaborated below, the correction is not small so that the NSWC code has an advantage. Also, base drag coefficients predicted by this code are in good agreement with the flight data of Stoney.[6]

III. POST PROCESSING

Since the NSWC code does not accept inlets, the tangent ogive cowl, in the computational model, is extended to form a closed, pointed nose. Assuming that slender body theory is valid for the nose extension, no correction is made for the normal-force slope as the contribution,

$$C_{N\alpha i} = 2\left(\frac{D_i}{D}\right)^2 \tag{1}$$

is equal to that predicted by momentum change of the ingested stream-tube. Furthermore, it is assumed that the contribution of the actual cowl to C_{N_α} is the same as with nose extension. The center-of-pressure, however, is shifted backward. The amount of shift depends on the structure of the shock and expansion waves within the inlet. Since this is not known at present, a conservative assumption is used, namely that the above contribution acts at the inlet plane. Approximating the foremost part of the extended nose by a cone, having a length l_e, the change in pitching moment coefficient is:

$$\begin{aligned} \Delta C_{M\alpha i} &= -\frac{1}{3}\,\frac{l_e}{D}\,C_{N\alpha i}\,, \\ &= -\frac{2}{3}\,\frac{l_e}{D}\left(\frac{D_i}{D}\right)^2\,. \end{aligned} \tag{2}$$

The associated shift in center-of-pressure is:

$$\Delta\left(\frac{X_{cp}}{D}\right) = -\frac{2}{3}\,\frac{l_e}{D}\left(\frac{D_i}{D}\right)^2\,\frac{1}{C_{N\alpha}}\,. \tag{3}$$

The roughness elements, required by sabot launch, generate additional drag that depends on geometry, Mach and Reynolds numbers and flight conditions. The additional drag reduces the dynamic pressure of the flow approaching the fins. It is expected that the reduced dynamic pressure will decrease the efficiency of the fins as stabilizers.

The full treatment of the problem is a topic for computational fluid dynamics. Here, an engineering approximation is proposed, for use in conjunction with the design code.

The drag coefficient of the roughness elements can be estimated based on correlations of experimental data such as by Hoerner[7] and Young and Patterson;[8]

$$\Delta C_A = 4\frac{h}{D} C_{D_e}^s \tag{4}$$

where the superscript s refers to a series of protuberances or grooves, considering the interference between the elements.

The additional axial-force appears as an increase in boundary-layer momentum thickness

$$\Delta\delta^{**} = \frac{D}{8}\Delta C_A = \frac{1}{2} hC_{D_e}^s \quad . \tag{5}$$

The thickening of the boundary layer also causes an increase in the displacement thickness, $\Delta\delta^*$. In the case of the 60mm SFRJ-FINNER, that will be discussed in the next chapter, the thickness of the boundary-layer ahead of the roughness is very small compared to the increase due to the threads. It is assumed that the shape factor over the rough surface is the same as that over a smooth one. The shape factor, $H = \Delta\delta^*/\Delta\delta^{**}$,depends on the velocity and density distribution. A common assumption is the validity of the 1/7 power law at supersonic Mach numbers and adiabatic flow. This assumption will be employed in the analysis that follows.

The displacement thickness, with roughness elements, is not small compared to the diameter of the body or the exposed span of the fins. Two aerodynamic effects are produced by the thickened boundary layer. The first one is the flaring of the center-body to an effective diameter $D_i = (D + 2\Delta\delta^*)$. The contribution of the effective flare to normal-force curve slope, as predicted by slender body theory is:

$$\Delta C_{N\alpha f} = 2\left[\left(\frac{D_i}{D}\right)^2 - 1\right] \quad .$$

In the present case, only the actual cylindrical body carries normal loads. Hence, the above expression will be multiplied by the ratio of the cylinder projected area to that of the effective flare. Introducing the effective flare diameter, the additional contribution of the body due to roughness is:

$$\Delta C_{N\alpha t} = 2\left[\left(\frac{D+2\Delta\delta^*}{D}\right)^2 - 1\right]\frac{D}{D+\Delta\delta^*} = 8\frac{\Delta\delta^*}{D} \quad .$$

The second effect is the reduction of the contribution of the fins to the normal-force due to masking by the body boundary-layer. It is assumed that the inner sections of the fins, with width equal to $\Delta\delta^*$, become inefficient. The mask area on a pair of fins is $S_m = 2C_R\Delta\delta^*$. Thus, the contribution of a fin set to the normal-force and the pitching-moment is reduced by a factor

$$\eta = \frac{S - S_m}{S} \quad , \qquad (6)$$

$$\equiv 1 - 2\frac{C_R\,\Delta\delta^*}{S} \quad .$$

The corrected normal-force curve slope and the center-of-pressure location are

$$C_{N\alpha}{}^{+} = C_{N\alpha b} + \eta C_{N\alpha f} + \Delta C_{N\alpha t} \quad ,$$

$$C_{M\alpha}{}^{+} = C_{M\alpha b} + \eta C_{M\alpha f} + \Delta C_{M\alpha i} + \Delta C_{M\alpha t} \quad ,$$

$$\frac{X_{cp}}{D}^{+} = -\frac{C_{M\alpha}{}^{+}}{C_{N\alpha}{}^{+}} \quad .$$

IV. APPLICATION

1. 40mm SFRJ PROJECTILE

The external dimensions of the spin stabilized 40mm SFRJ configuration are shown in Figure 1. The truncated ogival nose has a fineness ratio of 1.8 and the cylindrical center body a fineness of ratio 2.4. The inlet diameter ratio is $D_i/D = 0.51$.

The computed normal-force curve slope and center-of-pressure are shown in Figure 2a and Figure 2b, respectively. The Van Dyke method predicts a smaller lift carry over than that

predicted by the SOSE method. It shows as a smaller normal-force slope and a more forward center-of-pressure. The correction for the inlet opening, relative to the computational model that has an extended nose, amounts to a backward shift of center-of-pressure of about 0.045 calibers.

Comparison of the prediction with range flight data,[9] and wind-tunnel data,[10] is also presented in Figure 2. The measured slope of the normal-force curve is 18-23% higher than that calculated. Thus, the experimental Aircraft DATCOM[11] data base is used for further validation of the analysis. This empirically based source, substantiates the results of the SOSE method, for extended nose body, down to a Mach number of 1.5. It is concluded that the cowl produces more normal-force with an open inlet than with an extended nose. It should be noted that the range data is an average of 15 tests with large scatter and an estimated error in excess of 30%.

The data obtained in free flight shows an average center-of-pressure location which is 0.08 calibers more aft than that predicted. The wind-tunnel data are in near perfect agreement with the analysis at low Mach numbers and gives up to 0.24 calibers in a more aft location at the high end of the Mach number range.

2. 75mm SFRJ PROJECTILE

The 75mm SFRJ is a spin stabilized projectile having a nose fineness ratio of 2.0 and a center body fineness ratio of 1.6. The inlet diameter ratio is 0.474 (also see Figure 3).

The analytically computed normal-force curve slope and center-of-pressure are presented in Figure 4a and Figure 4b, respectively. Here, the correction to the pitching-moment coefficient shifts the center-of-pressure backward about 0.04 calibers. As in the case of the 40mm projectile, no boundary layer displacement thickness corrections were applied.

The agreement between the predicted static aerodynamic coefficients and those obtained at a Mach number 4.44 in ballistic range tests[12] is very good, as is apparent in Figure 4. The experimentally obtained normal-force curve slope is only 3.7% higher than that predicted and the center-of-pressure location is 0.1 calibers more forward.

3. 60mm SFRJ-FINNER PROJECTILE

The 60mm SFRJ-FINNER projectile, shown in Figure 5, is sabot launched. The truncated ogival nose has a fineness ratio 1.63 and the inlet diameter ratio is $D_i/D = 0.5745$. The center body has fineness ratio 5.60 and features four pairs of buttress threads. Two sets of fins were used, as shown in Figure 5a and Figure 5b. The original one has aspect ratio of 0.92 and the extended one aspect ratio of 0.528. Both sets have the same exposed span which is 0.9745 body diameters.

As mentioned in Chapter II, the main difference between the two candidate codes is in the influence coefficient. This difference is illustrated in Figure 6 for the present configuration with original fins at Mach numbers of 2 and 4. The fin influence coefficient, $K_{T(B)}$, is assumed independent of the fin over-hang by the DATCOM code. On the other hand, the NSWC code predicts a decrease in the coefficient as over-hang ratio increases. The body influence coefficient, $K_{B(T)}$, predicted by the NSWC code is somewhat smaller than that predicted by the DATCOM code. Both codes assume that this influence coefficient diminishes as the square of one minus the over-hang ratio. The sum of the two influence coefficients predicted by the NSWC code is about 15% lower than that predicted by the DATCOM code.

A step in the validation of the code was a comparison of computed body alone characteristics with data bases. The Aircraft DATCOM,[11] used in Section 1, and the ESDU[13] data bases were used. The comparison, for the extended nose body, is shown in Figure 7. The analysis is in excellent agreement with the data bases at Mach numbers between 2.0 and 3.0. The code underpredicts the normal-force curve slope by 6.7% at Mach number of 1.5 and by 8.3% at 5.0. The predicted center-of-pressure location is 0.1 calibers more forward than that predicted by the data base at a Mach number of 1.5 and 0.14 calibers at 5.0. To summarize this comparison, as in the case of the 40mm SFRJ, the data bases corroborate the prediction by the SOSE method down to a Mach number of 1.5.

The drag coefficient of the buttress threads was estimated using the empirical data compiled by Young and Patterson.[8] It is assumed that the drag produced by each thread is a sum of a chamfered forward facing step and that of a backward facing one. Each of these contributions depend upon flight conditions and the smooth wall skin friction. Since data is limited, the dependence on Mach number is based on that of a straight ridge. For this protuberance, it was found, from Figure 4.37 of Reference 8, for $1.4 \le M \le 2.8$ that the drag coefficient ratio for a constant Reynolds number is:

$$\frac{C_{D_e}(M)}{C_{D_e}(2)} = \left(\frac{M}{2}\right)^{-0.43} \quad . \tag{7}$$

Since no data were found for $M > 2.8$, this expression was used up to $M = 5.0$. The drag coefficient curve of a single thread, based on frontal area, C_{D_e}, was evaluated for two flow conditions. One is for full-scale flight at sea level, assuming that the surface reaches recovery wall temperature; the other is for NASA Langley Research Center (LaRC), unitary wind-tunnel, where tests, which will be described in the following chapter, were performed. The estimates are presented in Figure 8 and show that the drag coefficient of a single thread under the LaRC wind-tunnel flow conditions is much smaller than that in free flight. This difference is caused by the large difference in Reynolds number between the two cases.

The contributions of the eight threads in series is evaluated using the empirical data of Lacey, reported in Figure 4.46 of Reference 8. It is estimated that for the present average ridge density and surface length to ridge height ratio, the drag of the series is 3.74 times that of a single isolated thread. It is assumed that this factor is independent of Mach number. The additional axial-force coefficient, due to the series is evaluated using Equation (4) and presented in Figure 9 for the two flow conditions described above.

As mentioned above, the boundary layer shape factor is based on the assumption of the validity of the power law at supersonic Mach numbers and adiabatic conditions, and that it is unaffected by surface roughness. These assumptions were validated by comparing experimentally obtained data by Fenter[14] (sand roughness, $1.62 < M < 2.70$) and Voisinet[15] (screens, $M = 2.95$) to the analytical results of Shapiro.[16] The agreement is good and the differences between smooth and rough wall cases are small, as shown in Figure 10.

The momentum thickness, associated with the additive drag due to the buttress threads, decreases as Mach number increases, as shown in Figure 11. For the free-flight case, the displacement thickness increases with Mach number and reaches a value of 0.05 bodies diameters at $M = 5.0$. For the LaRC flow conditions, δ^* decreases as the Mach number increases and its value at $M = 5.0$ is 0.017 body diameters. The associated fin efficiencies is shown in Figure 12. For $M = 5.0$, which is the design Mach number, the fin efficiencies at flight conditions are 0.83 and 0.87 for the original and extended fin configurations, respectively. The difference between the two cases is due to the variance in their aspect-ratios and the taper ratios. In the LaRC flow conditions, the fin efficiency is very close to 1.0, reflecting the small axial-force due to the buttress threads.

Figure 13 shows the predicted aerodynamic characteristics of the configuration having the original fins in free-flight conditions. The code predicts instability at Mach numbers larger than 2.0. A range test at a Mach number of 4.25 showed that this configuration is indeed unstable. The broken lines between Mach numbers 1.5 and 2.0 indicate computational transition from the use of a transonic method to the use of supersonic lifting surface method in the evaluation of fin alone characteristics. In the present case, the code uses the value $C_{N_\alpha} = \pi AR/2$, as predicted by slender wing theory, for Mach numbers for which $AR\beta < 2.0$. The jump between this value and that predicted by supersonic lifting surface method is not physical. It is expected that the actual curves will be more smooth than those predicted by the code.

Results of the analysis for the configuration having the extended fin, under free-flight conditions, are shown in Figure 14. The normal-force curve slope (Figure 14a) with buttress threads is almost equal to that of the smooth body for Mach numbers smaller than 3.5 and slightly higher at Mach numbers larger than 4.0. The forward shift of center-of-pressure (Figure 14b) due to the threads reaches a value of 0.20 calibers at a Mach number of 5.0. The analysis predicts a very

small margin of stability for a smooth body and instability at Mach numbers larger than 4.3 for the rough one.

Results of one range flight test were available at the time of preparation of this report. The measured center-of-pressure falls between the two predicted curves. The measured normal-force curve is nine percent higher than that computed.

V. WIND-TUNNEL TEST OF THE 60mm SFRJ-FINNER PROJECTILE

1. OBJECTIVES

The objectives of the two sets of wind-tunnel tests, that will be described in this chapter are:

1. To determine the margin of static stability of the 60mm SFRJ-FINNER projectile as a function of Mach number.

2. To determine the effects of the buttress threads on SFRJ projectile stability.

3. To determine the effect of ingested inlet flow on normal-force and stability.

4. To calibrate current design codes in terms of their ability to predict SFRJ projectile aerodynamic characteristics.

Other factors considered, such as grooves versus buttress threads, fin over-hang and fin size were tested but will not be considered here.

2. EXPERIMENTS

The NASA Langley Research Center (LaRC) Unitary wind-tunnel is an asymmetric, 4 ft. by 4 ft. test section, facility. The test plan by Yalamanchili[17] called for force and moment measurements at five Mach numbers between 3.0 and 4.6 with stagnation conditions adjusted to give a Reynolds number per foot of 2×10^6. The model was basically a full scale 60 mm SFRJ with buttress threads. A second model was tested with the space between the threads filled so as to produce a smooth continuous body shape. Tests were also performed with an extended nose attached, eliminating the flow through the model. A six component internal strain gauge balance was used with sting mounting of the model. When operated with an open inlet, the flow was believed swallowed although Schlieren photography failed and was not available.

The US Army Chemical Research, Development and Engineering Center (CRDEC) tests by Olsen et. al.[18] were performed in the Aerodynamics Research and Concepts Assistance Branch

supersonic wind-tunnel. This tunnel is also an asymmetric, blow down tunnel with a 6 in. by 6 in. test section. The tunnel was operated at lower but overlapping Mach numbers (2.00 to 3.75) with respect to the LaRC experiment. The air supply conditions involved higher stagnation pressures so that the Reynolds number per foot were five times the Langley value. Because the CRDEC tunnel is considerably smaller, a 0.3175 scale model of the 60mm SFRJ configuration was employed. The model was also sting mounted with an internal strain gauge balance for measurement of normal-force and pitching moment.

Both facilities reduced their measurements to normal-force and pitching-moment coefficients versus angle of attack. It is assumed that sting deflection and instrument errors, if any, have been accounted for in the reduced data.

3. DATA ANALYSIS

The C_N vs α and C_M vs α data were analyzed by fitting an expression of the form

$$y = a + b\alpha + c\alpha|\alpha| \quad .$$

This equation was selected because it is the simplest, low order, formula which displays the general form observed and expected in the data. That is, ideally (perfectly symmetric model in uniform flow) the forces and moments are expected to be odd functions of α. However, some non-ideal behavior is observed in that the forces and moments do not, as a rule, go to zero at zero angle of attack. The values of a, b and c are determined by a least square technique. The best fit value of b is interpreted as the slope of the normal-force or pitching-moment coefficient curve, $\partial C_N/\partial\alpha$ or $\partial C_M/\partial\alpha$, depending on whether $y = C_N$ or C_M. The center of pressure is then calculated from these slopes:

$$\frac{X_{cp}}{D} = -\frac{C_{M_\alpha}}{C_{N_\alpha}}$$

where the X is measured from the reference point in the definition of C_M. The LaRC data referenced the moments to a point 0.5358L (L = 19.03 inches or the length of the closed inlet configuration) from the closed inlet nose. The CRDEC reference for moments is the model base. In the results reported here X_{cp} is referenced to the lip of the open cowl configuration even for the closed inlet case.

4. ACCURACY

The accuracy of the Langley balanee is cited as ±0.25 percent of full scale which, for each component, is ±0.25 lbf or ±0.5 lbf-in. for normal-force and pitching moment, respectively.

These values can be represented as percent uncertainties in N and M. For example, at $M_\infty = 3.0$ and $\alpha = 6^o$, N = 8.2 lbf ±3% and M = 14.4 lbf-in. ±3.5%.

An alternate evaluation of the uncertainties can be derived from the statistics of the curve fits. The analysis can be extended to all the aerodynamic characteristics (C_{N_α}, C_{M_α} *and* X_{cp}). From each curve fit an estimated standard deviation is calculated from:

$$\sigma_y = \left\{ \sum_{i=1}^{n} [y_i - (a + b\alpha_i + c\alpha_i|\alpha_i|)]^2/(n-3) \right\}^{1/2}$$

A plot of a sample C_N versus α and C_M versus α are given in Figure 15. These results are for $M_\infty = 3.00$, and a closed inlet configuration with buttress threads. The curve fits are shown as solid or dashed lines for the LaRC or CRDEC data, respectively. The estimated standard deviations for this typical case are:

	σ_{C_N}	σ_{C_M}
LaRC	0.0041	0.0045
CRDEC	0.013	0.039

Based on the averages of the estimated uncertainties of the LaRC and CRDEC results. The CRDEC data have three times more scatter and corresponding uncertainty. This difference can be directly attributed to the smaller scale of the model in the CRDEC experiment.

5. STABILITY OF THE 60mm SFRJ-FINNER PROJECTILE

Figure 16 shows the experimentally obtained center-of-pressure location of the 60mm SFRJ. Only the actual configuration, namely the one with open inlet and buttress threads, is included. In general, the LaRC and CRDEC results are in good agreement despite the significantly larger uncertainty in the CRDEC data. The center of gravity for this configuration is taken as 3.45 calibers. The static margin can be seen to be about 0.6 calibers at Mach number 2.00 and to decrease with increasing Mach number to about 0.2 calibers at Mach number 4.6.

One flight datum, from a limited number of ballistic range stations, seems to substantiate these wind-tunnel observations.

6. THE EFFECT OF WIND-TUNNEL STING

As mentioned in Chapter II, the NSWC design code takes into account the effect of fin overhang on the mutual wing-body influence coefficient. The analysis by this code represents free flight conditions. In the wind-tunnels, the models are held in place by sting balances that form an extension to the body. Since the diameter of the balances is smaller than that of the body, an air gap is formed between them and the over hanging fins. As a result, the analysis of the actual situation is complicated and can not be predicted by the design code. Hence, an upper limit for this effect is obtained by considering a configuration with the body extended to the trailing edge of the fins. The results are processed and only the effect of body on the tail is taken into account (the balance does not include the loads acting on the sting). The upper limit estimates for the increment in normal-force curve slope and the backward shift in center-of-pressure location, due to the balance, are shown in Figure 17. The shift in center-of-pressure location reaches 0.2 calibers, at Mach numbers larger than 4.0.

If the results of the wind-tunnel tests (Figure 16) are corrected, to exclude the effect of the sting on the fin, the static margin reduces to 0.5 calibers at Mach number of 2.0, vanishes at Mach number of 4.6 and becomes negative (unstable) at higher Mach numbers. These values should be considered conservative because the correction is an upper limit estimate for the difference between wind-tunnel and flight configurations.

7. COMPARISON WITH ANALYSIS

a. The axial-force coefficient Axial-force data is available only from the LaRC tests. The experimental contribution to this coefficient is obtained by

$$\Delta C_A = C_{A_{o_{BT}}} - C_{A_{o_{SMOOTH}}} .$$

The data for the extended nose configuration was used. A comparison with the predictions, described in Chapter IV, Section 3, is presented in Figure 18 and shows a good agreement. Recall that the comparison is valid for LaRC wind-tunnel conditions and that the full scale axial-force coefficient due to the buttress threads is expected to be much larger.

b. Effect of the buttress threads The analysis of the effect of the buttress threads on the normal-force and the pitching-moment coefficients assumes that the inner sections of the fins are masked by the boundary layer displacement thickness, associated with the additive axial-force caused by the threads. The results presented in Chapter IV, Section 3, are valid for free flight conditions. For the present comparison, the analysis was repeated for the LaRC wind-tunnel conditions with the pertinent fin efficiency shown in Figure 12. The slope of the normal-force curve is practically independent of the roughness. The predicted forward shift in the center-of-

pressure is 0.1 calibers at Mach numbers of 3.0, reducing to 0.05 calibers at a Mach number of 5.0. These changes are much smaller, especially for high Mach numbers, than those predicted for flight conditions.

The experimentally obtained normal-force curve slope is shown in Figures 19a and 20a for the open and closed inlets, respectively. No discernable effect of the buttress threads can be detected in either case. The effect of the buttress threads on the center-of-pressure location is shown in Figures 19b and 20b. The LaRC results show a 0.1 caliber improvement in static margin due to the buttress threads, in the case of the open inlet and no effect in the other case. On the other hand, the CRDEC results show a small forward shift in the center-of-pressure. Taking all the data, together with the uncertainties, it is concluded that there is a negligible effect of the buttress threads on the normal-force and pitching moment characteristics under these wind-tunnel conditions.

c. Effect of ingested inlet flow The analytic prediction of the SFRJ aerodynamic characteristics were based on the assumption that the normal force for the open inlet configuration is exactly the same as that of the extended nose configuration. This in turn is based on the observation that the force required to turn the ingested air is the same as the slender body prediction for the extended nose tip.

Figure 21 is a plot of the data discussed in the previous section, showing the effect of the open inlet on the aerodynamic characteristics. It is observed that the open inlet, with air flowing through the body, has a higher normal-force curve slope than that of the configuration with extended nose where the inlet is closed. The difference is about 0.49 at Mach number 2.0 and decreases as the Mach number increases. The experimentally obtained difference was fitted by

$$\Delta C_{N_\alpha}{}' = 0.73 - .124\,M \quad , \quad 2.0 < M < 4.6 \quad .$$

The center-of-pressure location with open inlet is 0.34 calibers more forward than that with the extended nose tip. This shift is practically independent of the Mach number.

$$\Delta\left(\frac{X_{cp}}{D}\right)' = -0.34 \quad .$$

The increment in pitching-moment coefficient, associated with the increment in the normal-force curve slope and the shift in-center-of-pressure is:

$$\Delta C_{M_\alpha}{}' = C_{N_{\alpha_e}}\left(\frac{\Delta X_{cp}}{D}\right)' - \left(\frac{x}{D}\right)_o \cdot \Delta C_{N_\alpha}{}' \quad .$$

The data were processed and the following curve was fitted to the results:

$$\Delta C_{M_\alpha}{}' = -0.34 + 0.35\,M \quad , \quad 2 \le M \le 4.6 \quad .$$

Within the range of interest, both $\Delta C_{M_\alpha}{}'$ and $\Delta C_{N_\alpha}{}'$ are positive, indicating that the center-of-pressure of the contribution due to the open inlet is upstream of the lip of the inlet. This implies that the additional load includes a couple.

d. Discussion The predicted aerodynamic characteristics of the 60mm SFRJ projectile having extended fins is shown in Figure 21, together with the experimental data discussed in the previous sub-section. On both ends of the Mach number range the experimentally obtained normal-force curve slope is higher than that predicted by 11% to 12%. The variation of the experimental data is monotonic and does not show a jump, as predicted by the NSWC code.

The experimentally obtained center-of-pressure location of the configurations having the extended nose tip are 0.25 to 0.40 calibers more aft than that predicted. Here, too, the change in location between low and high supersonic Mach numbers is gradual. The gaps in normal-force and center-of-pressure indicate that the contribution of the fins to static stability is slightly underestimated by the NSWC code.

The center-of-pressure location of the actual configuration, namely the one with the open inlet is in very good agreement with the prediction at Mach numbers under 2.5 and above 3.75. In the intermediate range the experimental curve is smooth. It appears that the effects associated with the open inlet offset the increased contribution of the tail.

VI. CONCLUSIONS

An hybrid method for the aerodynamic analysis of the SFRJ projectiles has been used on two spin stabilized and two fin stabilized configurations. The method uses the NSWC-Aeroprediction code for the analysis of a model configuration, having an extended nose and a smooth body. Engineering approximations are used to account for the aerodynamic effects of the inlet and the buttress threads.

The NSWC-Aeroprediction code was selected for the present work because it applies empirical corrections for the effect of fin over-hang on tail-body influence coefficients.

The predicted normal-force curve slope of the 40mm SFRJ is 18%-23% lower than experimentally observed. In the case of the 75mm SFRJ the difference is only 3.7%. The agreement in center-of-pressure location is very good in both configurations.

The hybrid method predicts that the 60mm SFRJ, with the original fins, is statically unstable at Mach numbers larger than 2.0. A transonic range test verified this prediction.

The analysis predicts that the 60mm SFRJ, with extended fins, has a static margin of 0.5 calibers at low supersonic Mach numbers. That diminishes as Mach number approaches 4.3, and becomes unstable at higher Mach numbers. Wind-tunnel tests of this configuration gave normal-force curve slope which is 11% to 12% larger than that estimated. The experimentally obtained center-of-pressure location is 0.15 to 0.20 calibers more aft than the analytical value. A study of the results show that the contributions of the open cowl to the normal-force is larger than estimated in the analysis and that the contribution of the fin set is slightly larger than predicted by the NSWC-Aeroprediction code.

The experimentally obtained contribution of the buttress threads to the axial-force coefficient is in good agreement with the predicted value. No effect of the threads on the stability of the projectile was observed. However, the expected effect in the wind-tunnel flow condition is within the accuracy of the measurements and is much smaller than that predicted for free flight conditions.

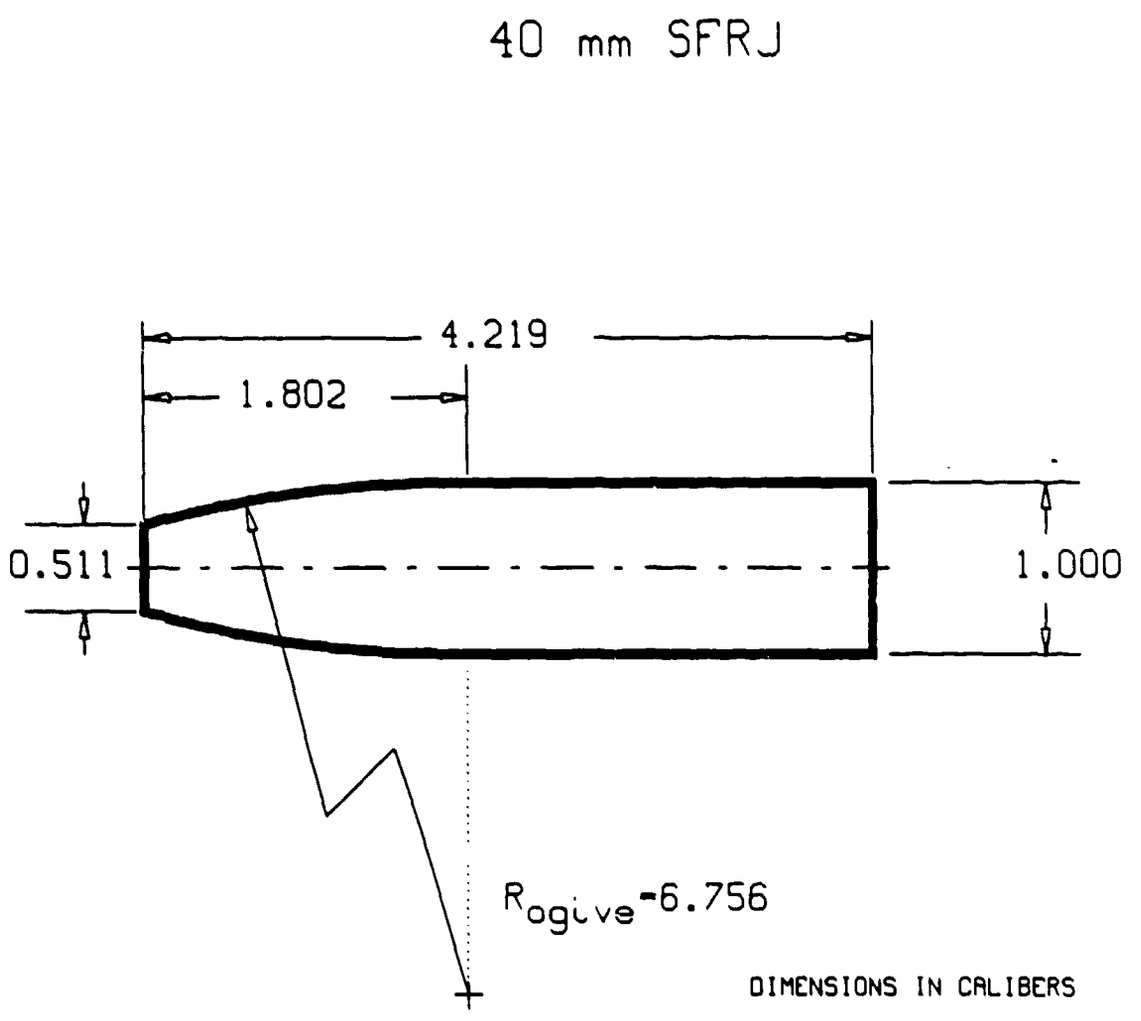

Figure 1. Geometry of the 40mm SFRJ projectile.

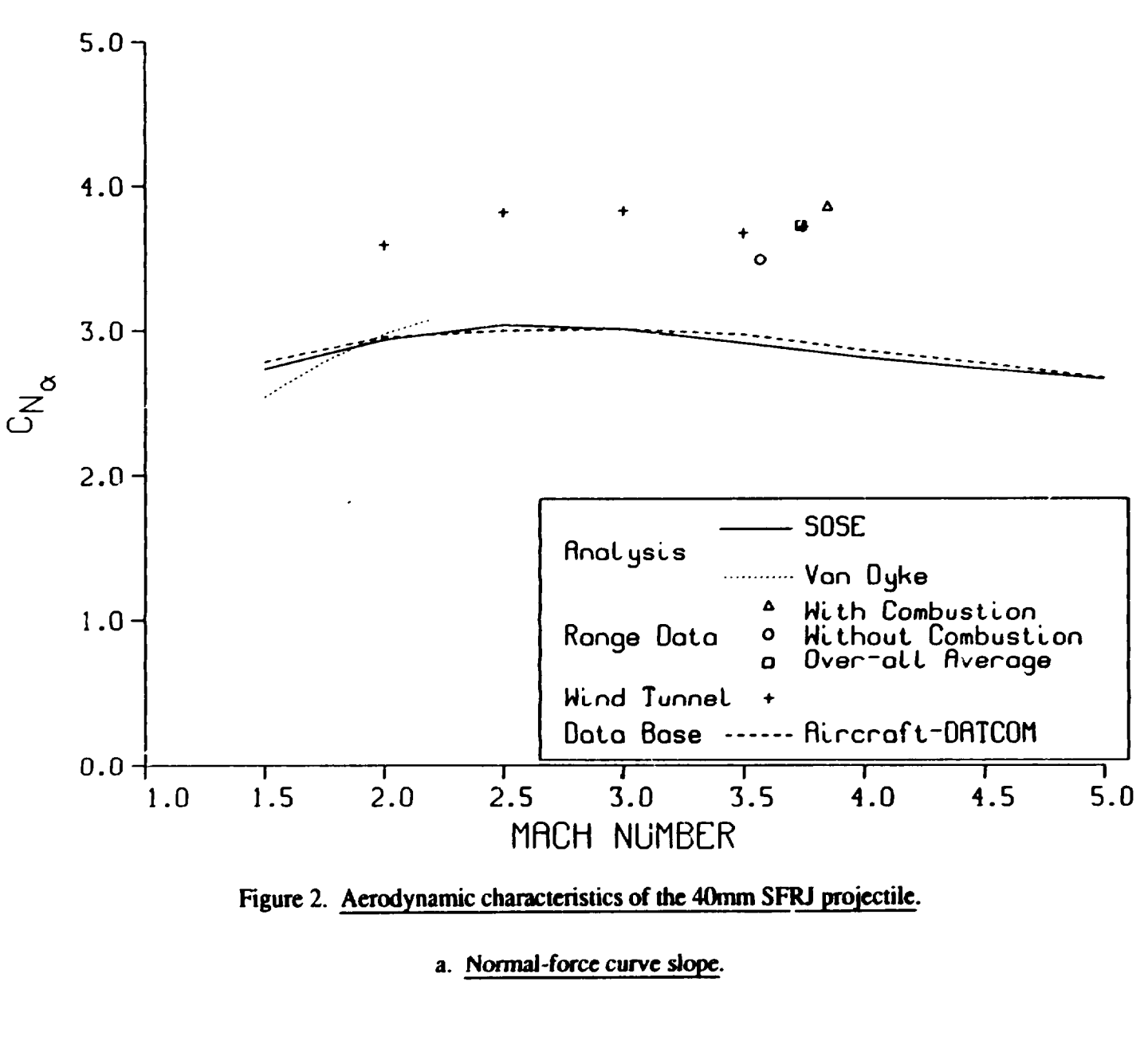

Figure 2. Aerodynamic characteristics of the 40mm SFRJ projectile.

a. Normal-force curve slope.

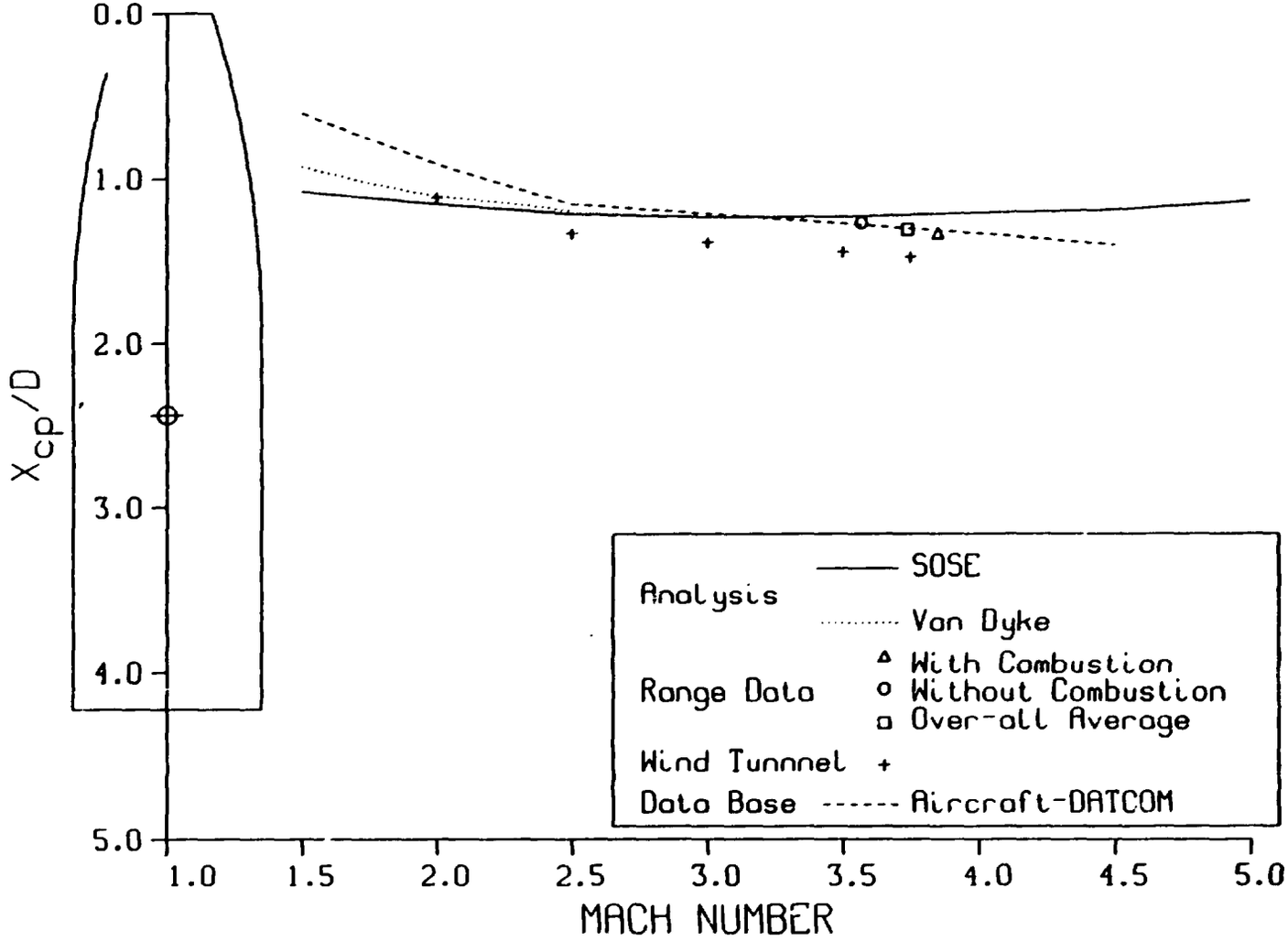

Figure 2. Aerodynamic characteristics of the 40mm SFRJ projectile.

b. Center-of-pressure.

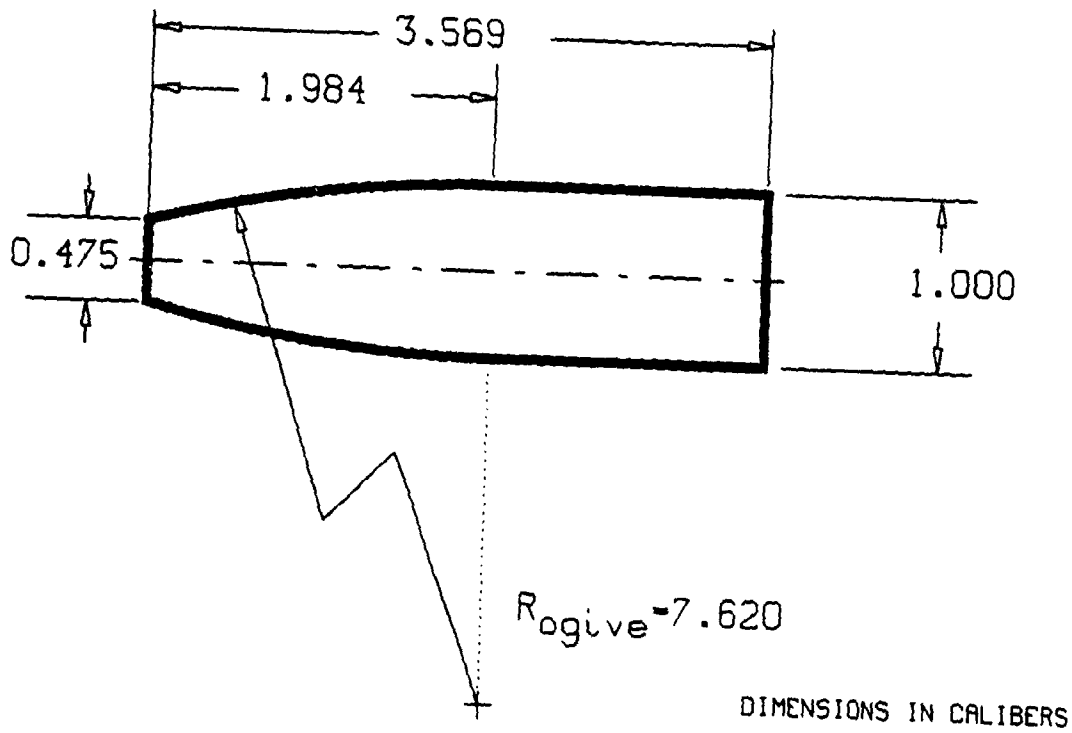

Figure 3. Geometry of the 75mm SFRJ projectile.

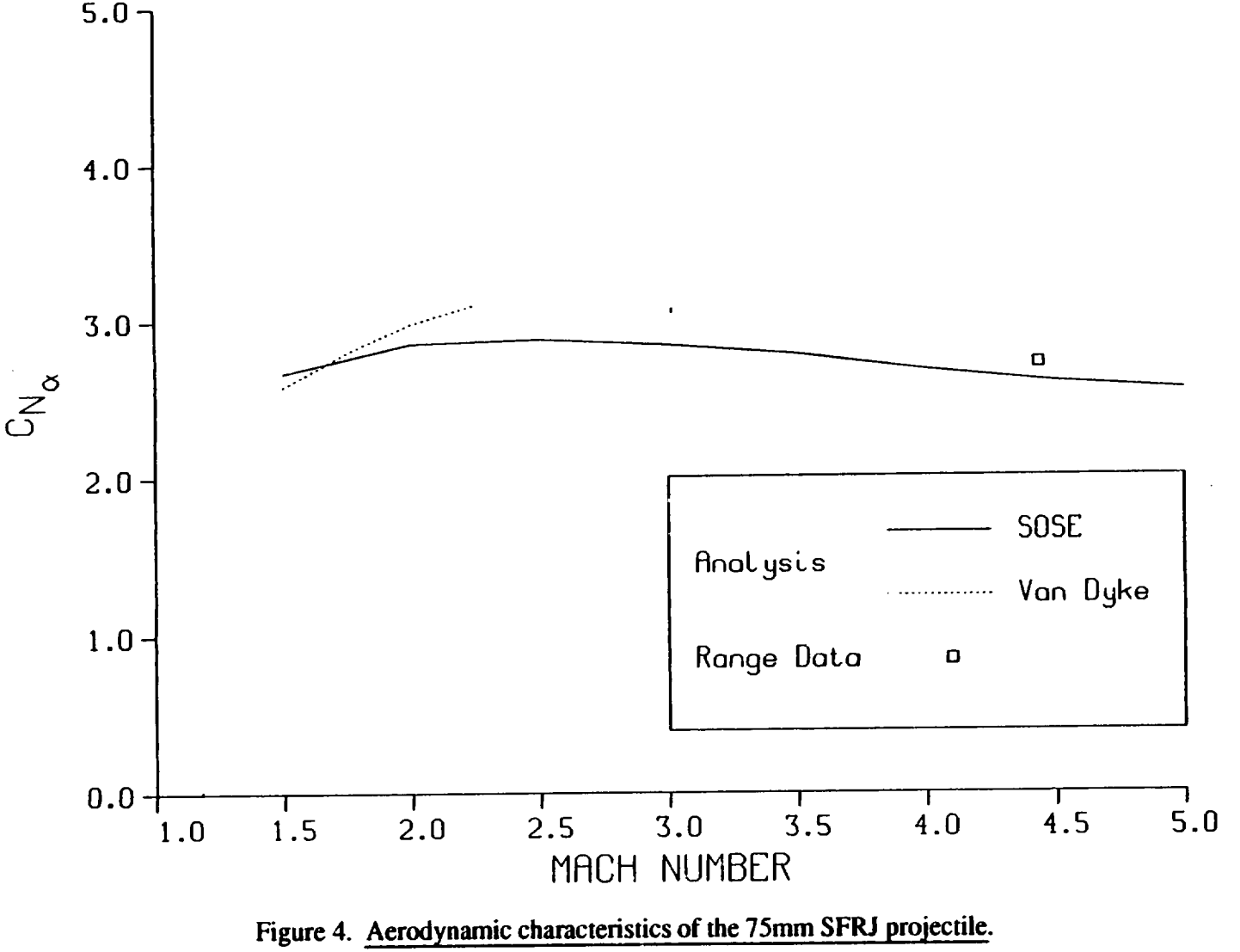

Figure 4. Aerodynamic characteristics of the 75mm SFRJ projectile.

a. Normal-force curve slope.

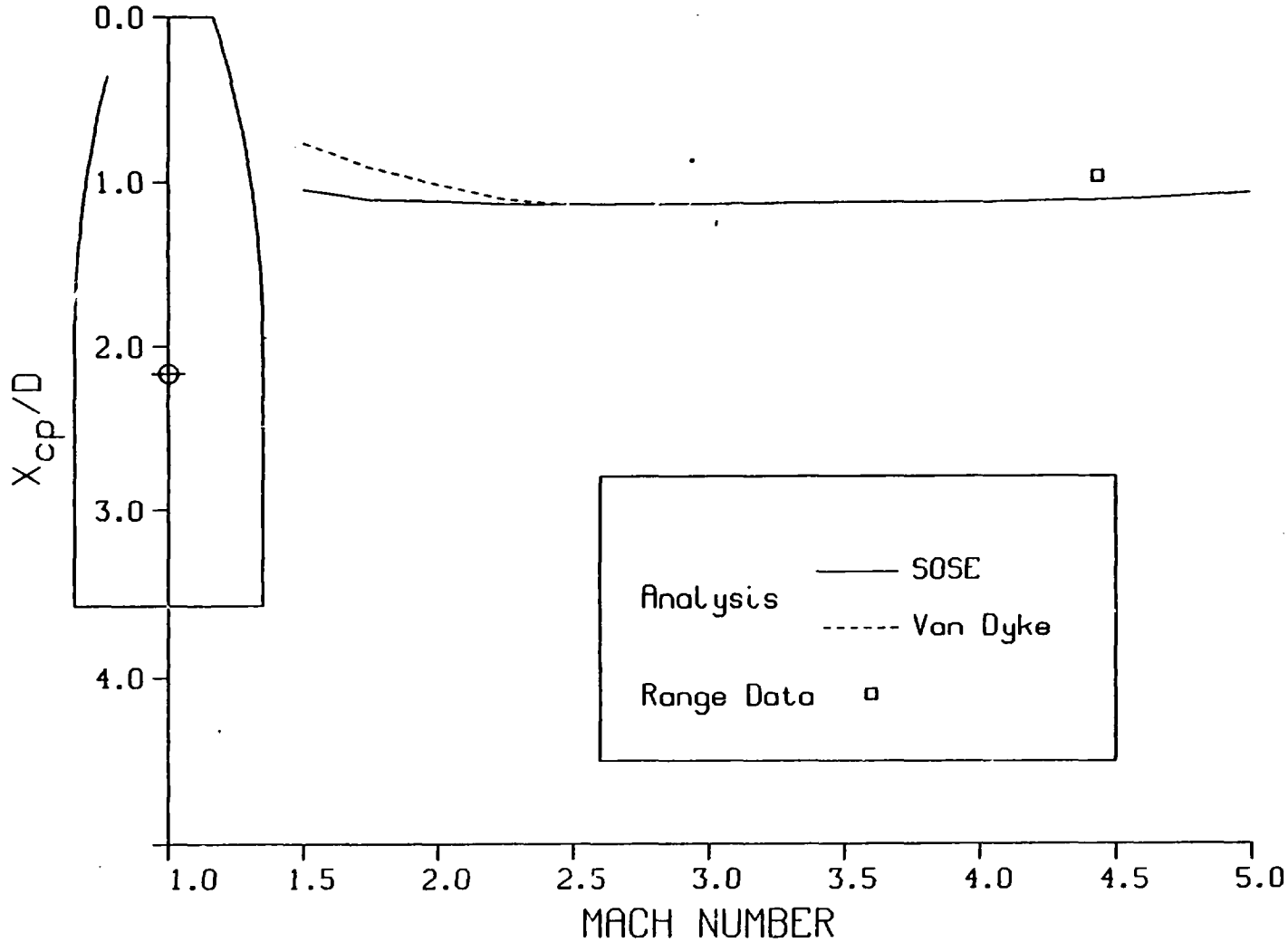

Figure 4. Aerodynamic characteristics of the 75mm SFRJ projectile.

b. Center-of-pressure.

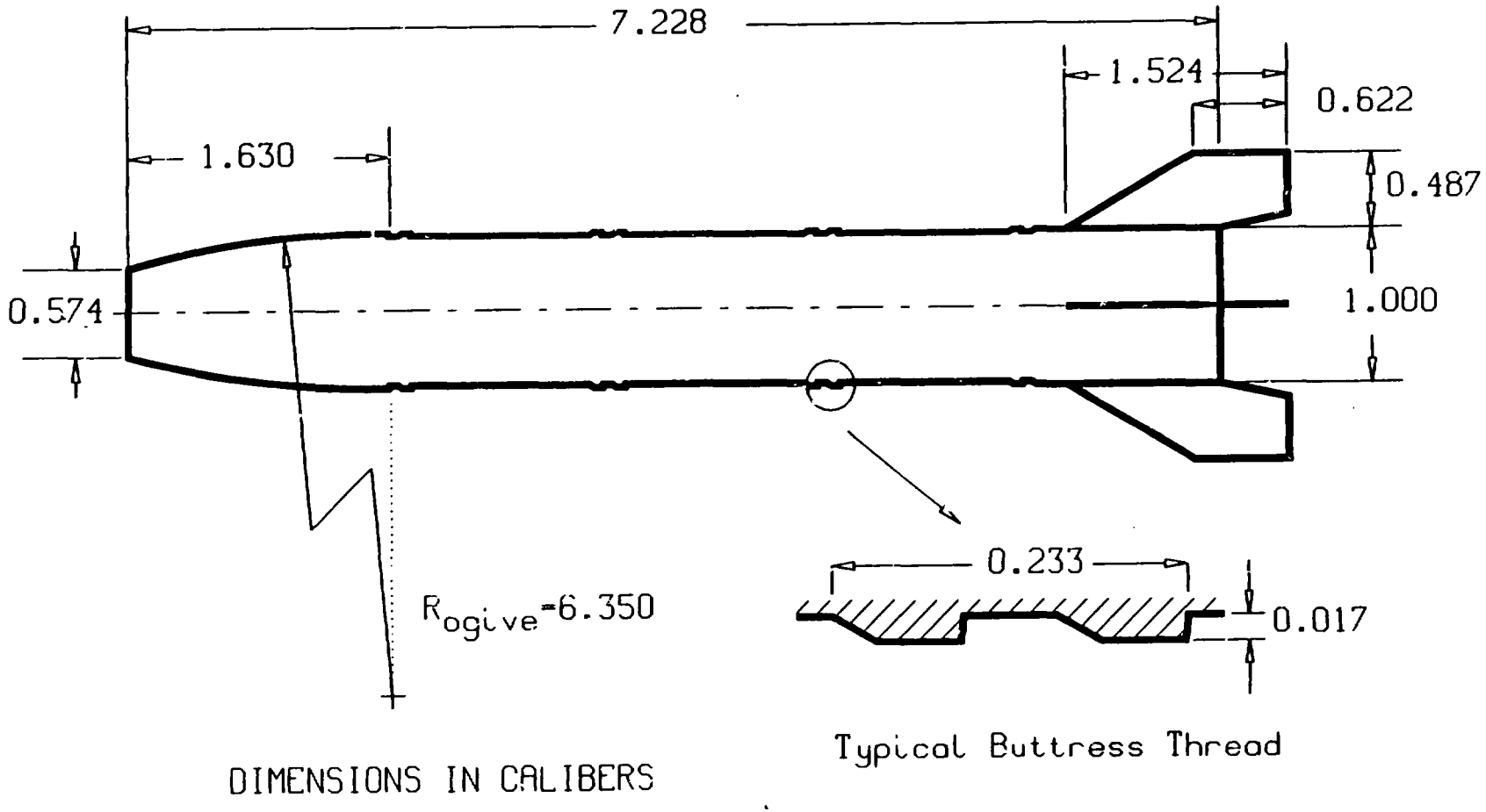

Figure 5. Geometry of the 60mm SFRJ projectile.

a. Original fins.

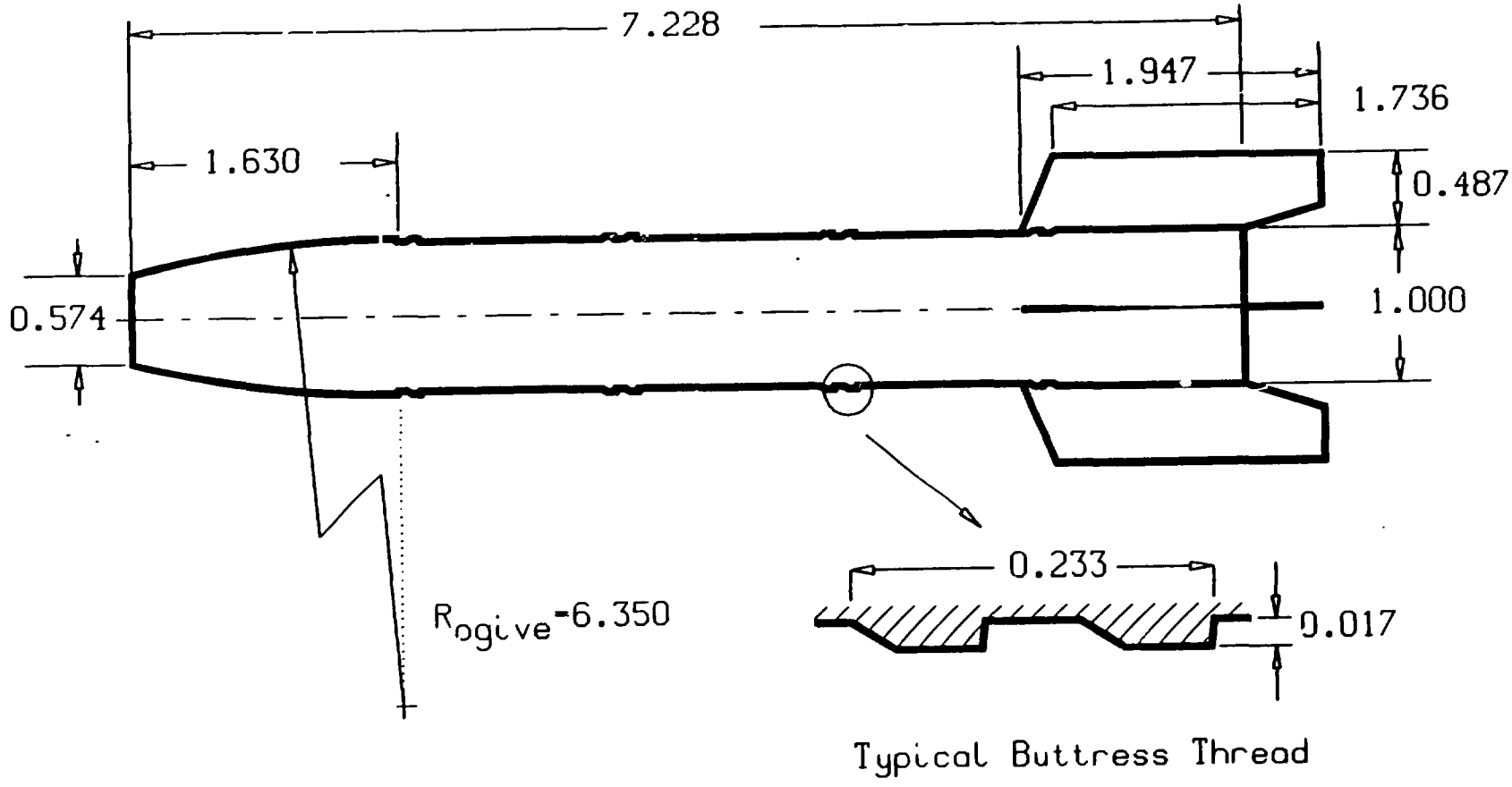

Figure 5. Geometry of the 60mm SFRJ projectile.

b. Extended fins.

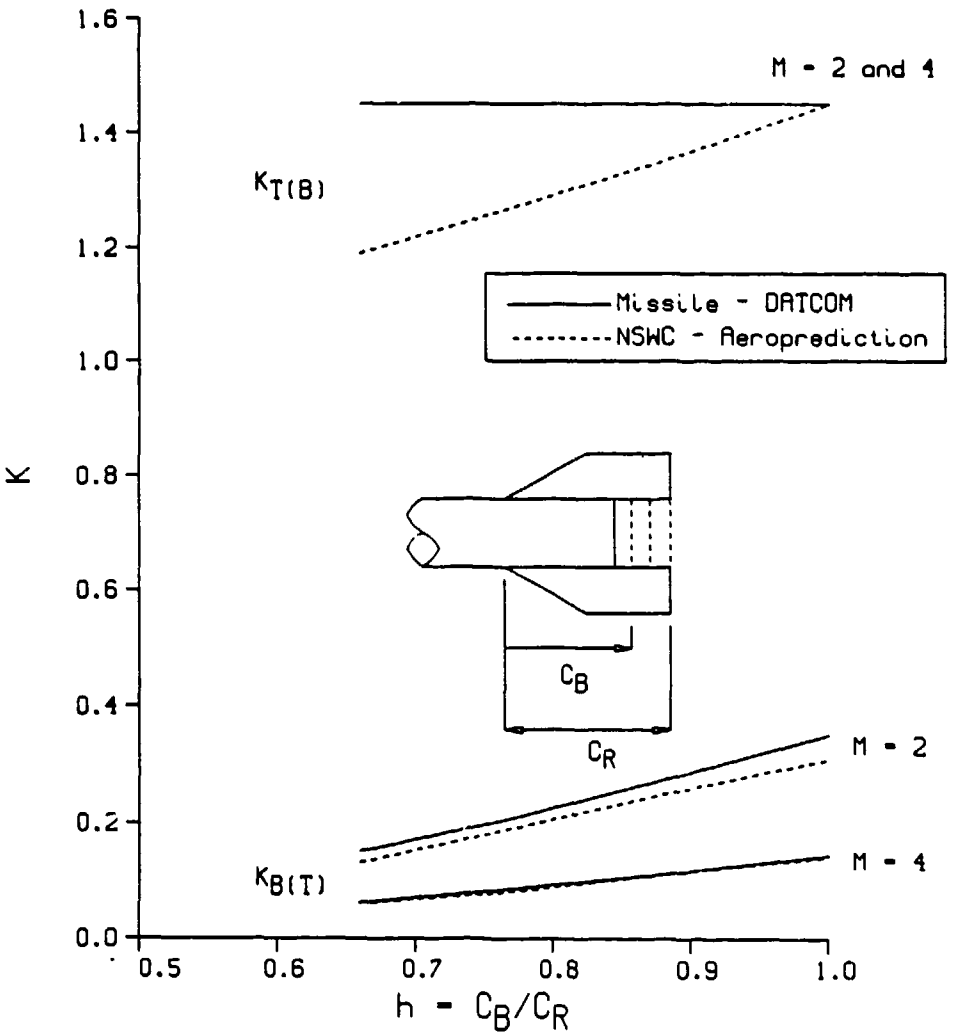

Figure 6. Dependence of the influence coefficients on over-hang.

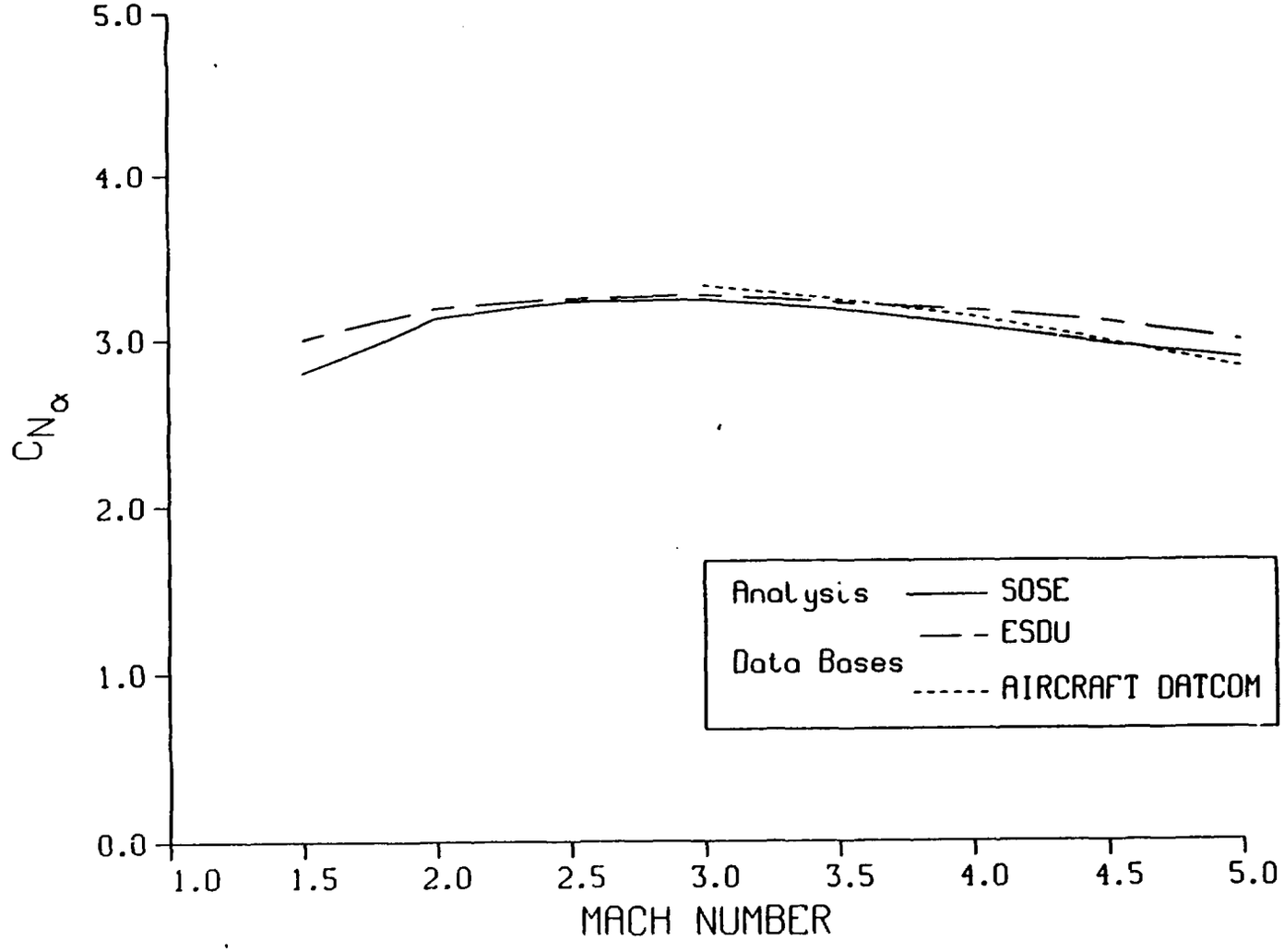

Figure 7. Aerodynamic characteristics of the body of the 60mm SFRJ projectile.

a. Normal-force curve slope.

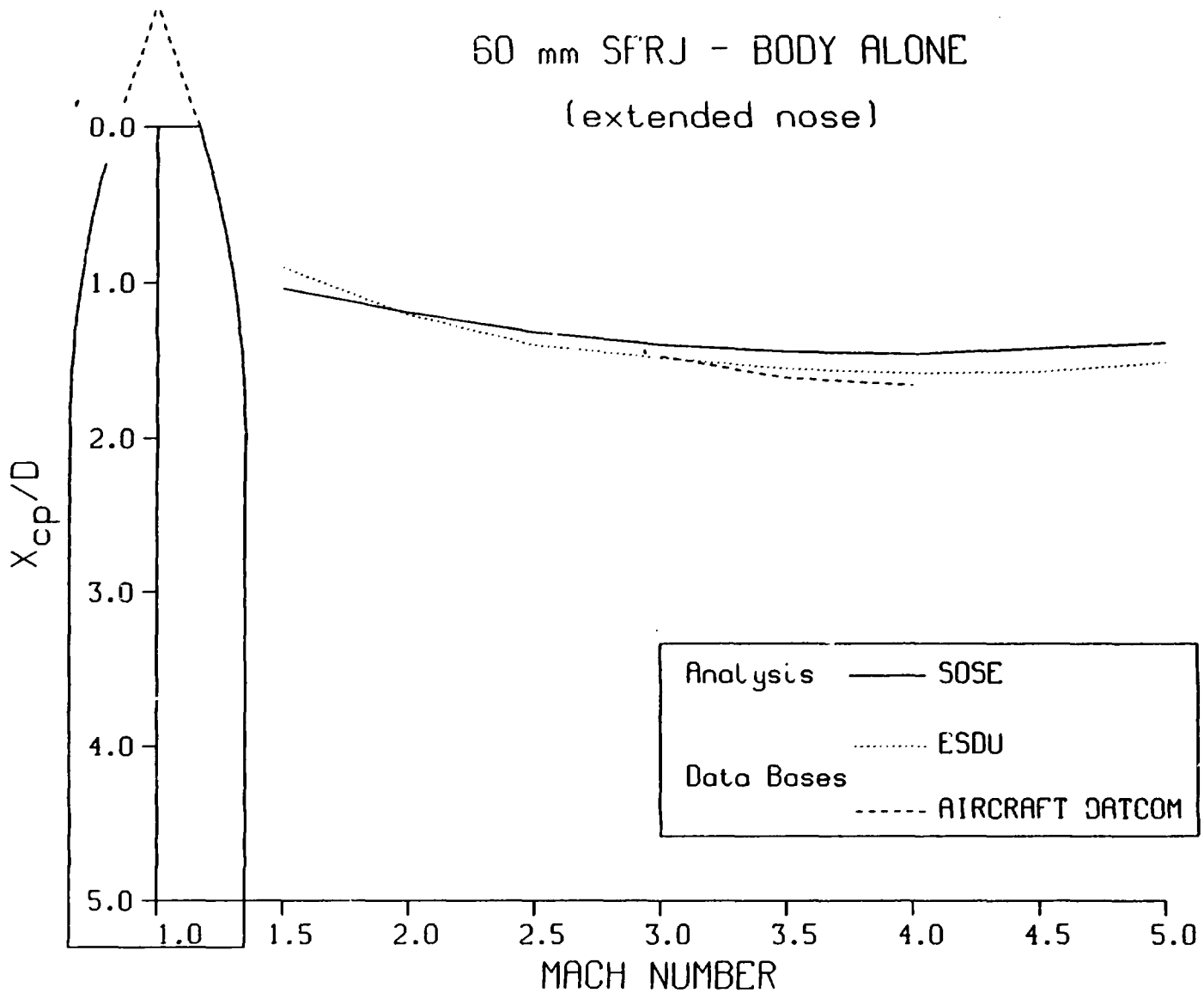

Figure 7. Aerodynamic characteristics of the body of the 60mm SFRJ projectile.

b. Center-of-pressure

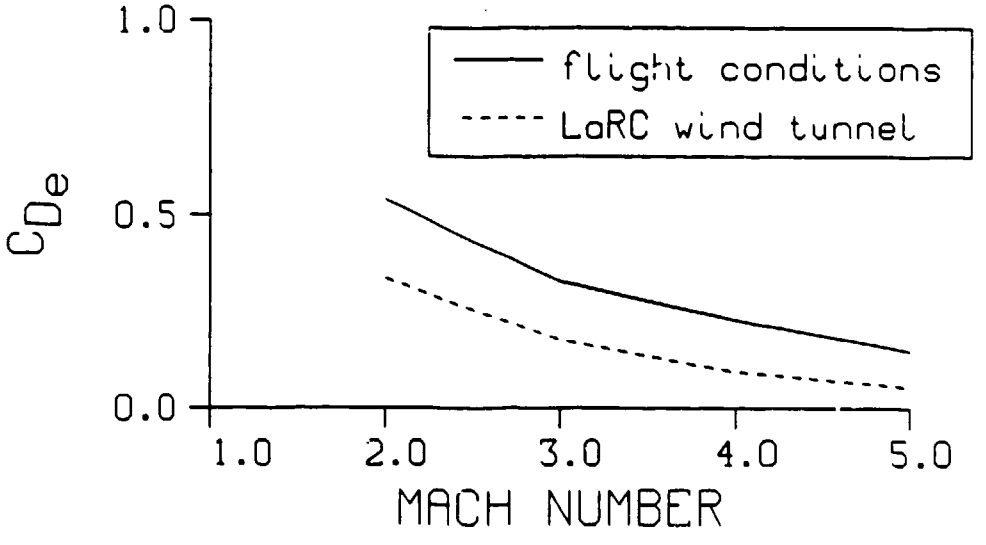

Figure 8. The drag of a buttress thread.

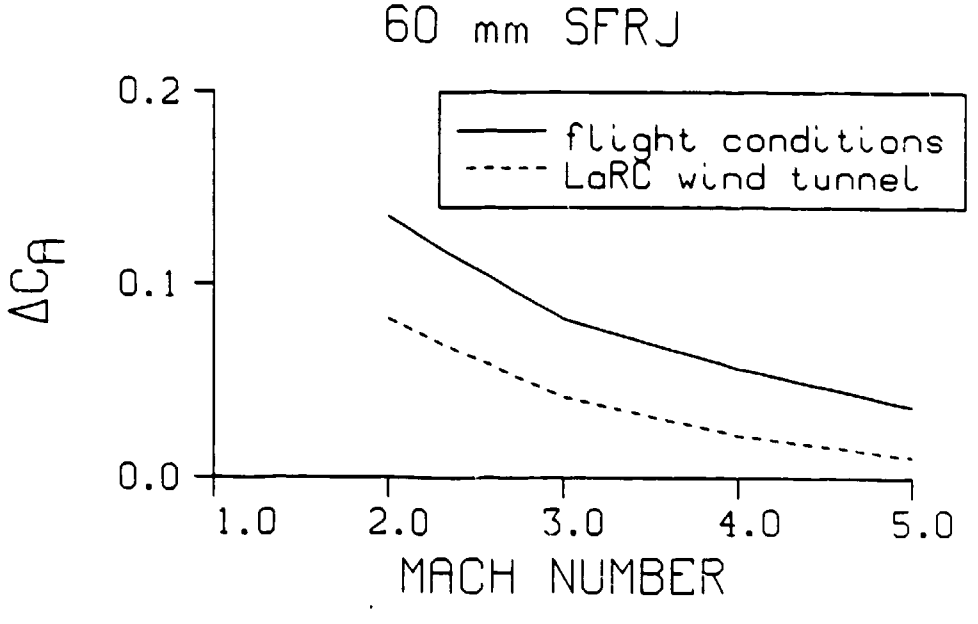

Figure 9. The additive axial-force coefficient due to the buttress threads.

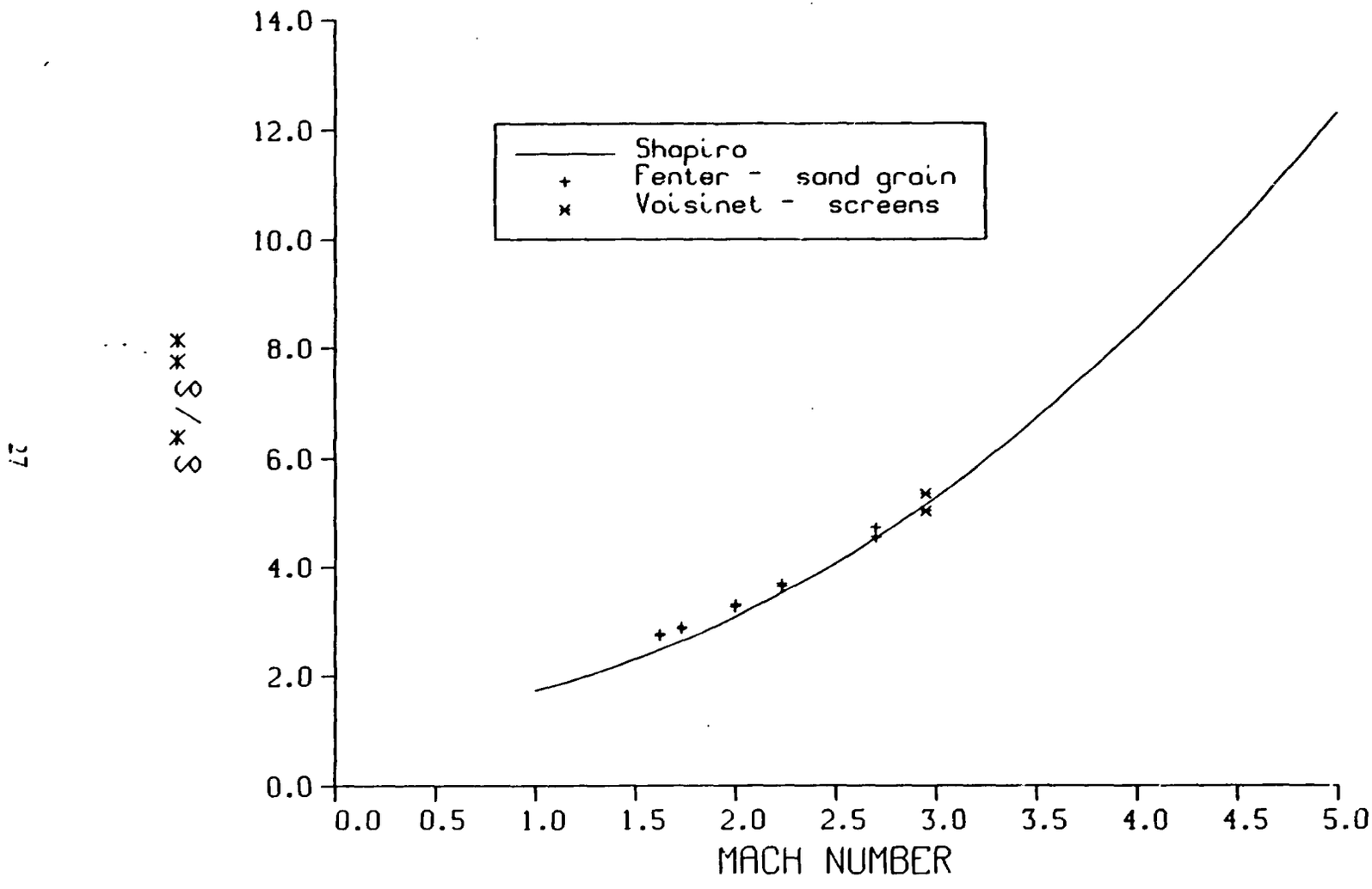

Figure 10. Comparison between experimentally obtained shape factor and analysis by Shapiro.

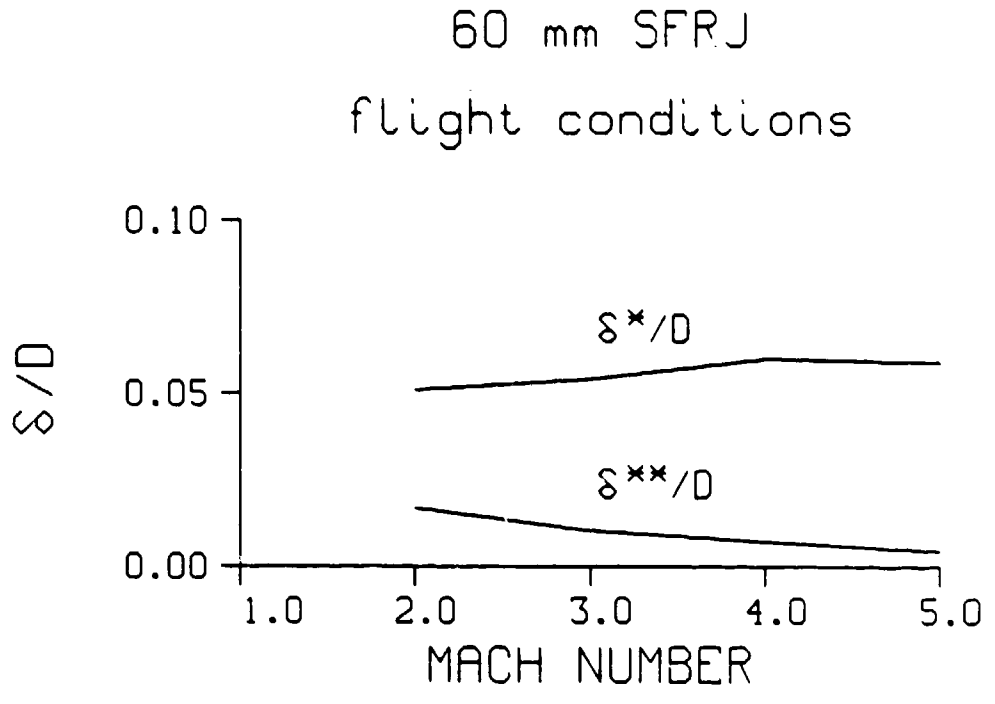

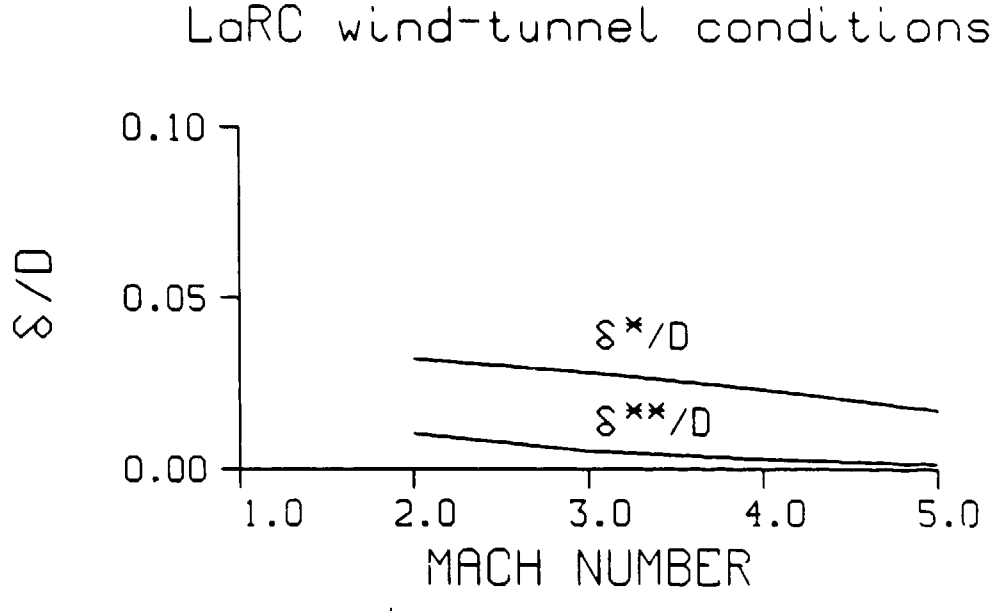

Figure 11. The increase in the integral boundary-layer thicknesses.

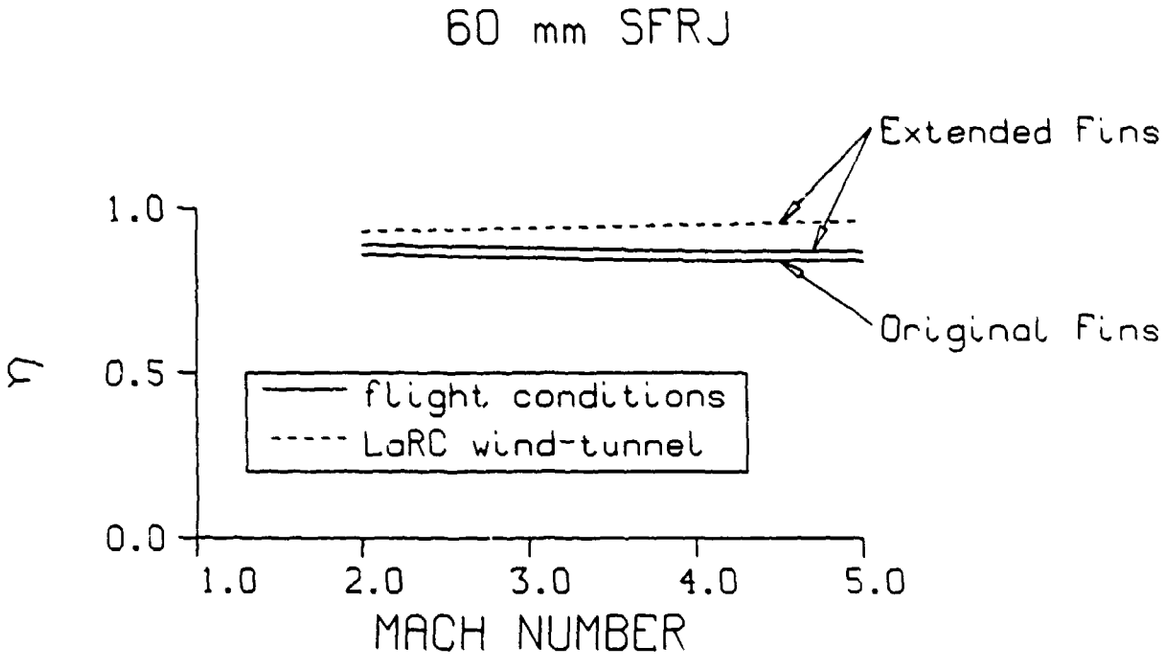

Figure 12. Fin efficiency.

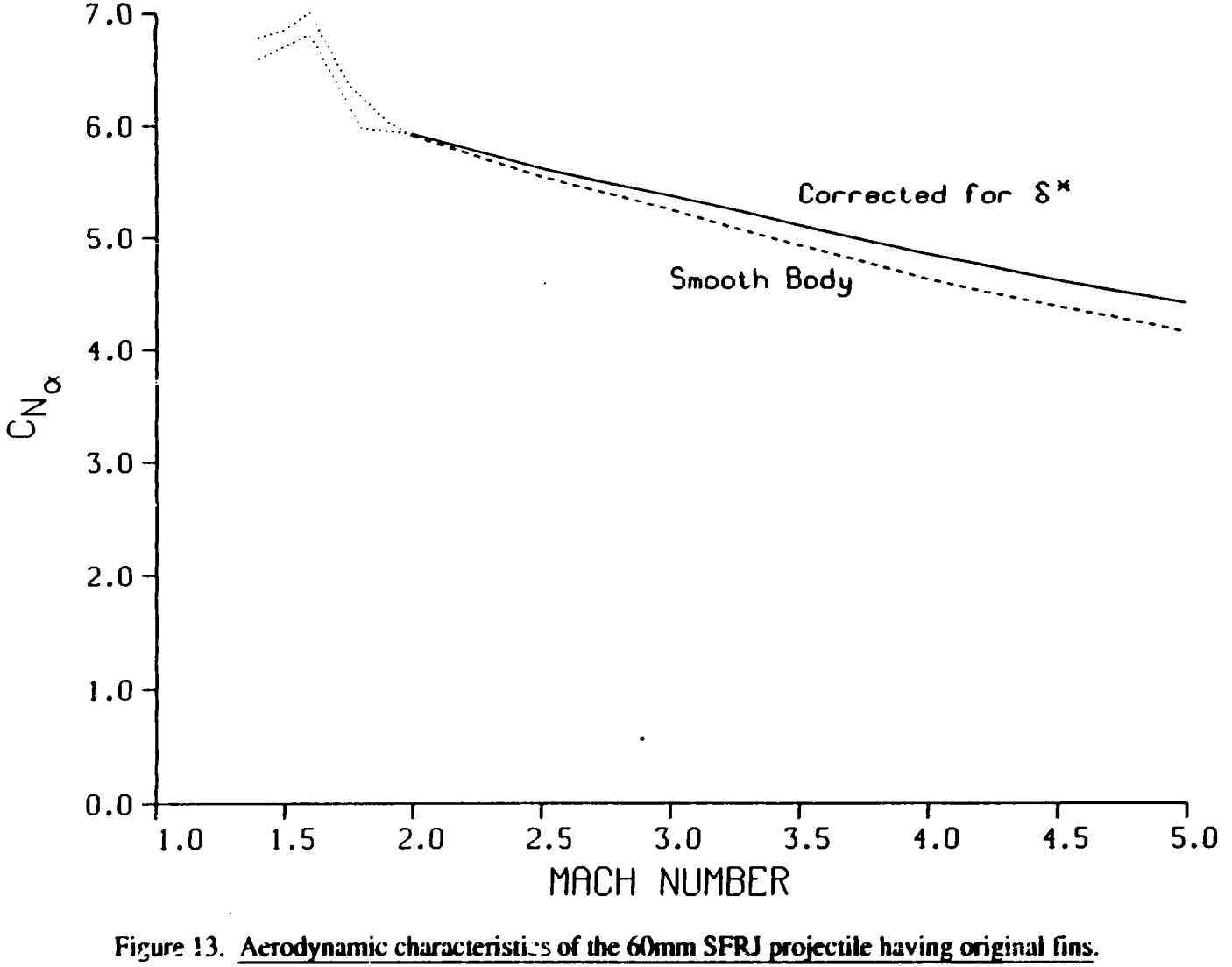

Figure 13. Aerodynamic characteristics of the 60mm SFRJ projectile having original fins.

a. Normal-force curve slope.

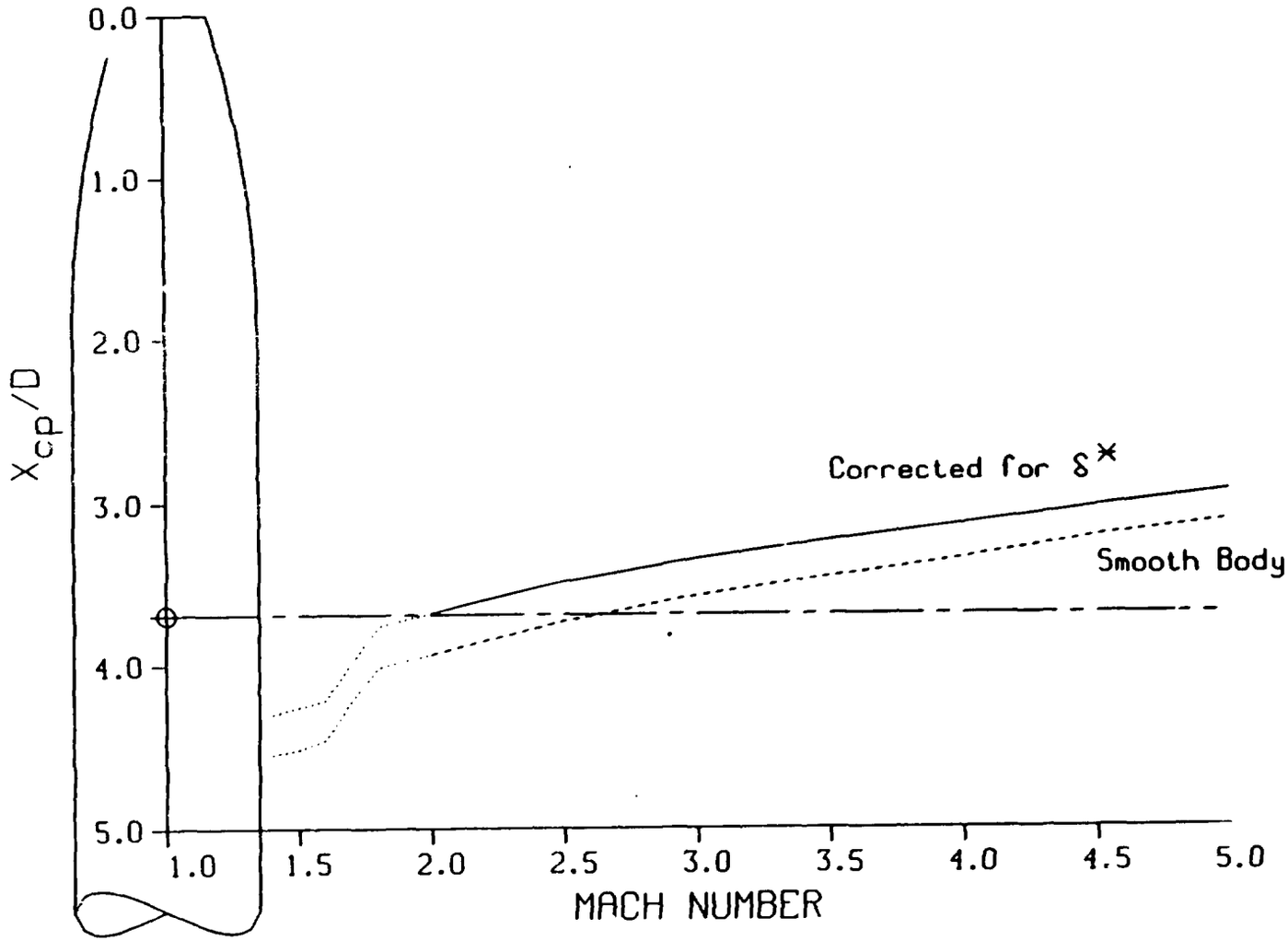

Figure 13. Aerodynamic characteristics of the 60mm SFRJ projectile having original fins.

b. Center-of-pressure.

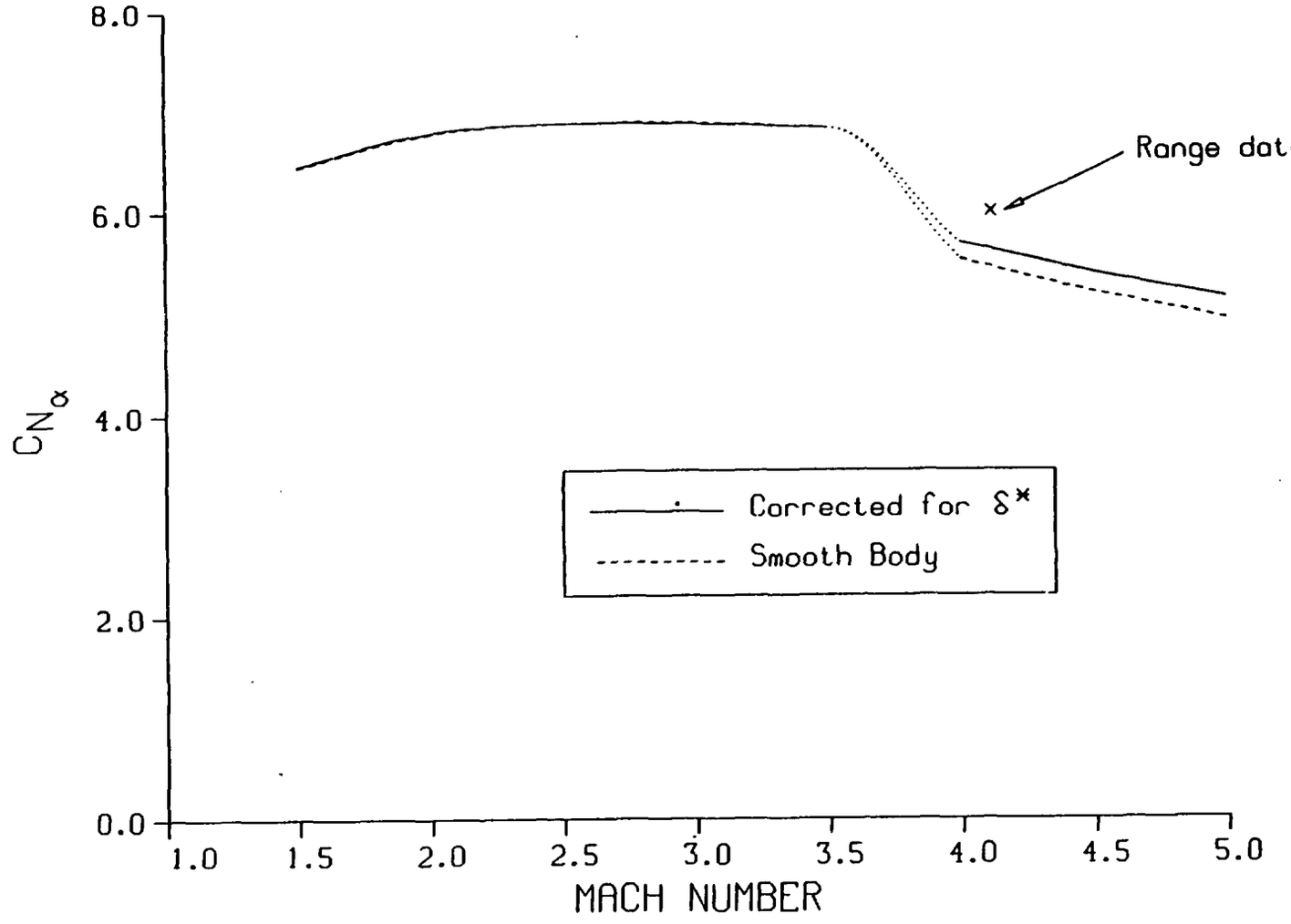

Figure 14. Aerodynamic characteristics of the 60mm SFRJ projectile having extended fins.

a. Normal-force curve slope.

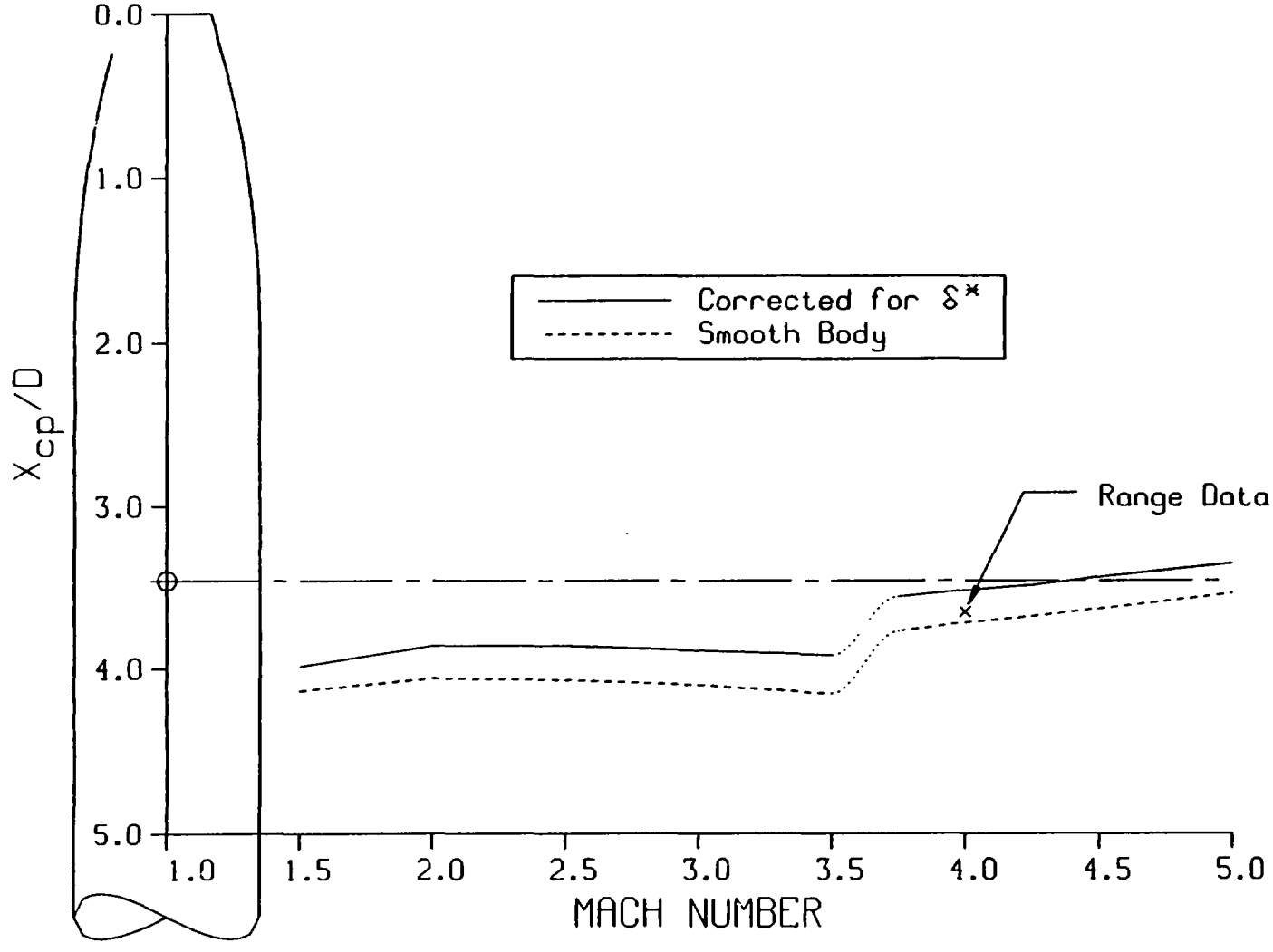

Figure 14. Aerodynamic characteristics of the 60mm SFRJ projectile having extended fins.

b. Center-of-pressure.

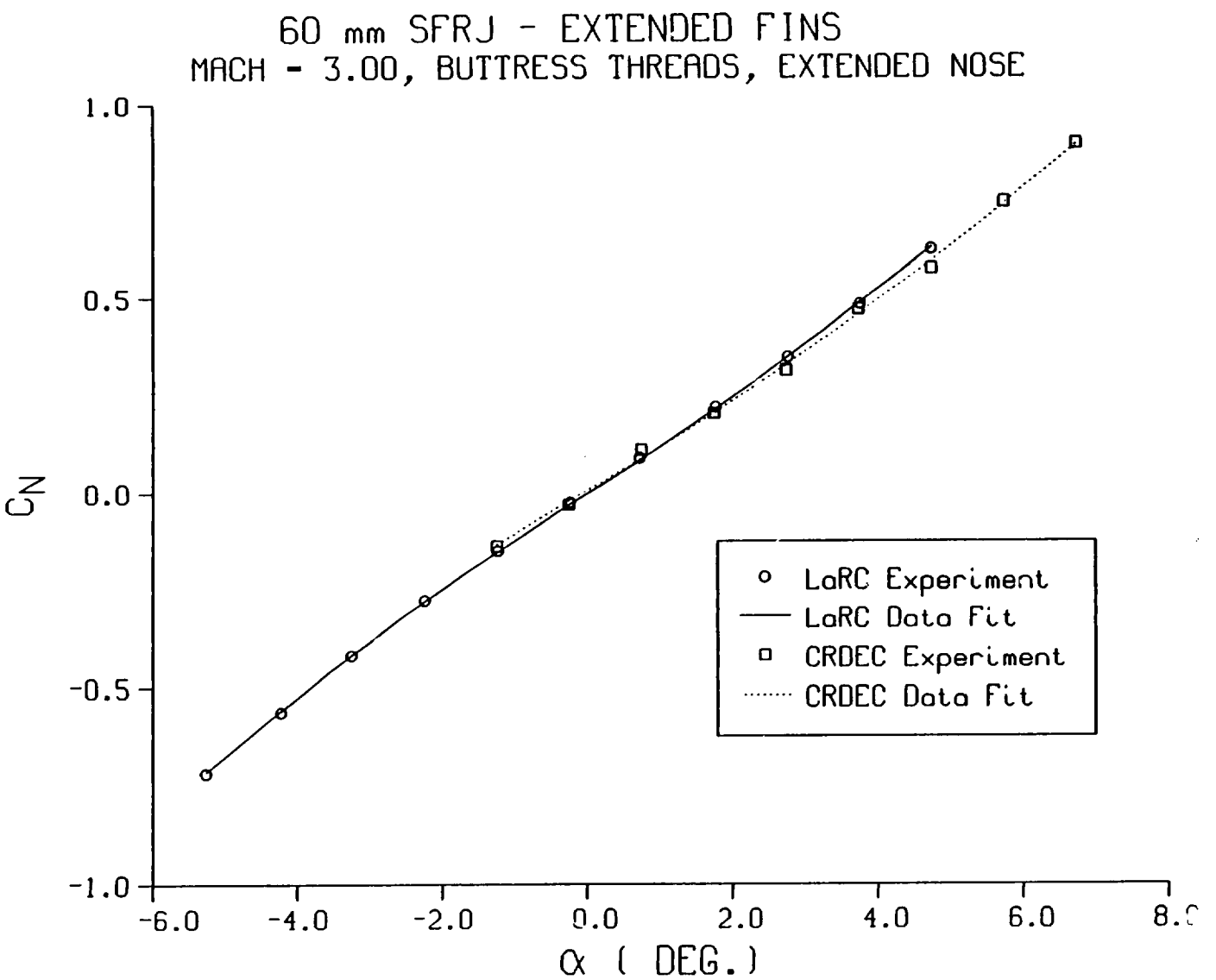

Figure 15. Comparison between LaRC and CRDEC data.

a. Normal-force coefficient.

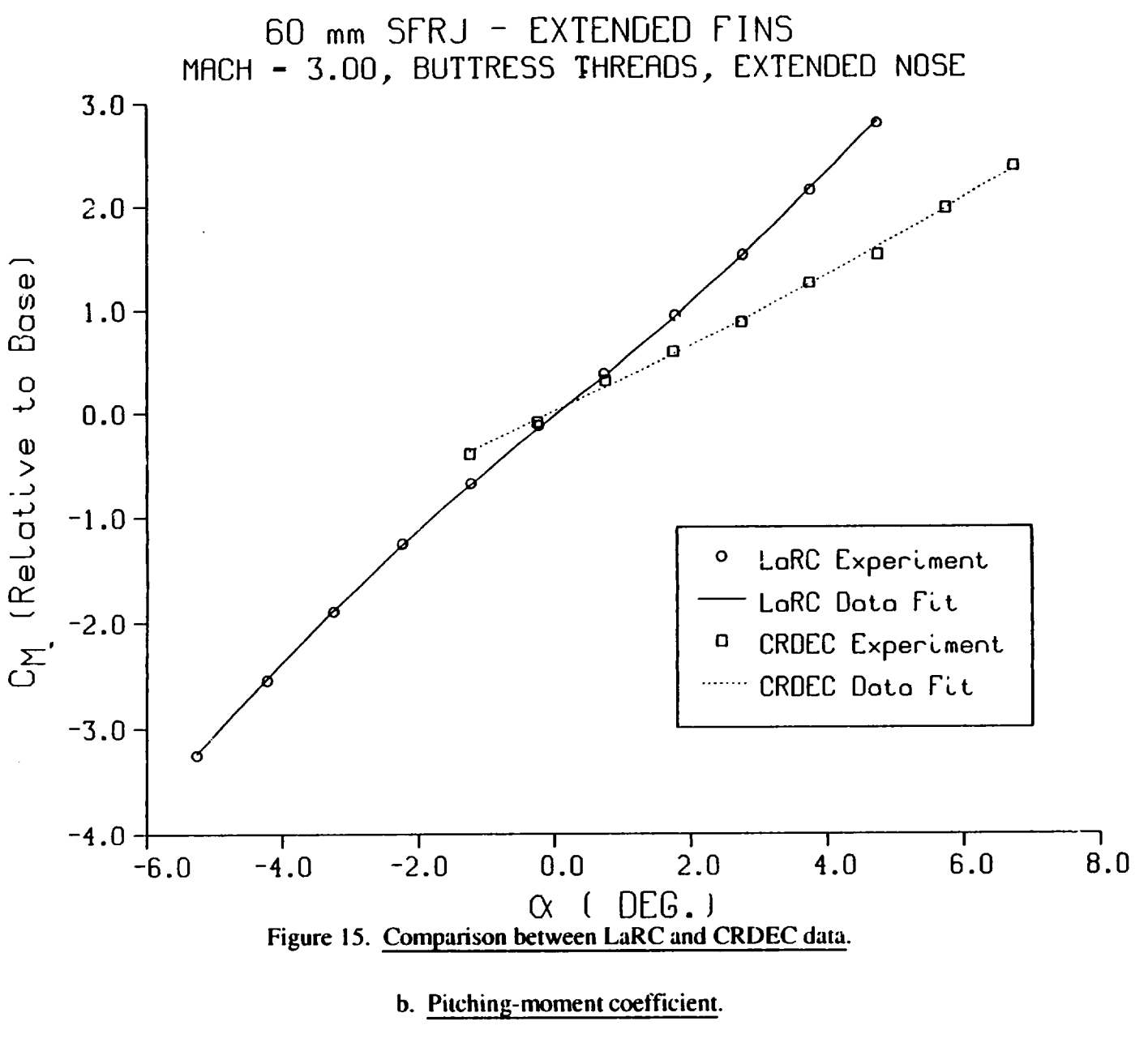

Figure 15. Comparison between LaRC and CRDEC data.

b. Pitching-moment coefficient.

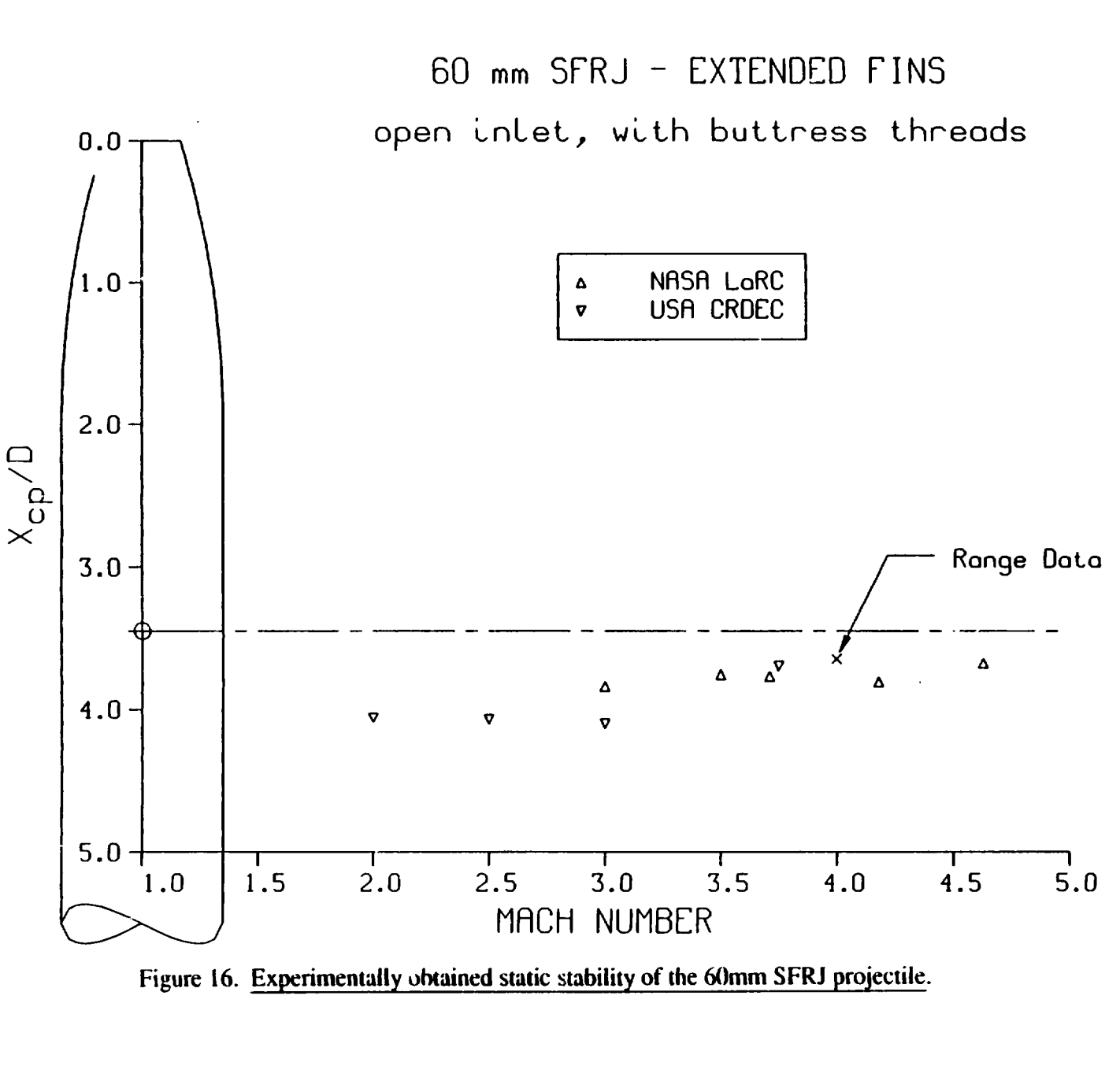

Figure 16. Experimentally obtained static stability of the 60mm SFRJ projectile.

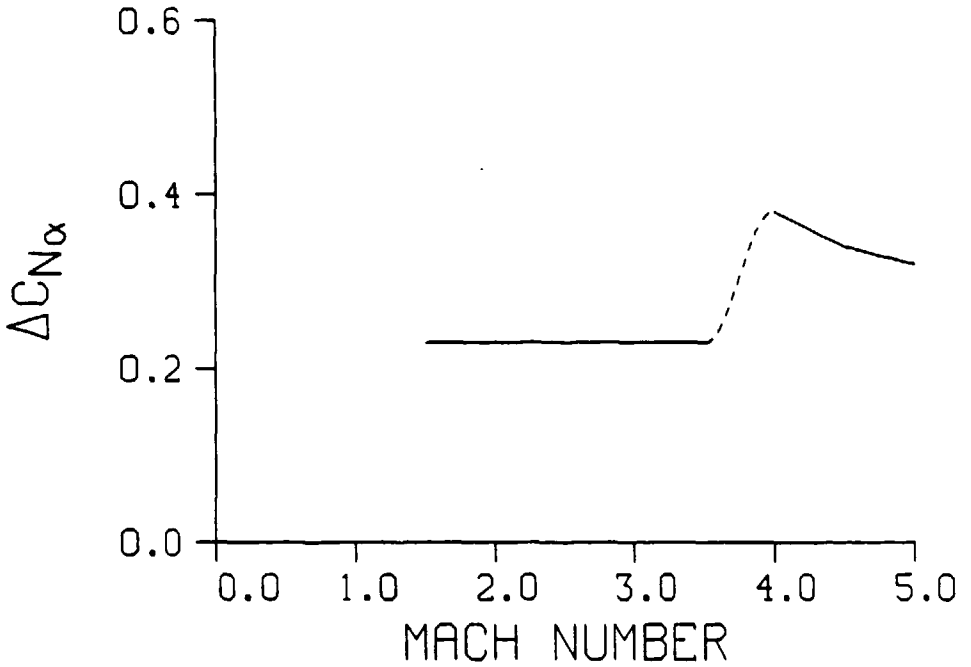

Figure 17. The effect of sting balance on the aerodynamic characteristics.
a. Normal-force curve slope.

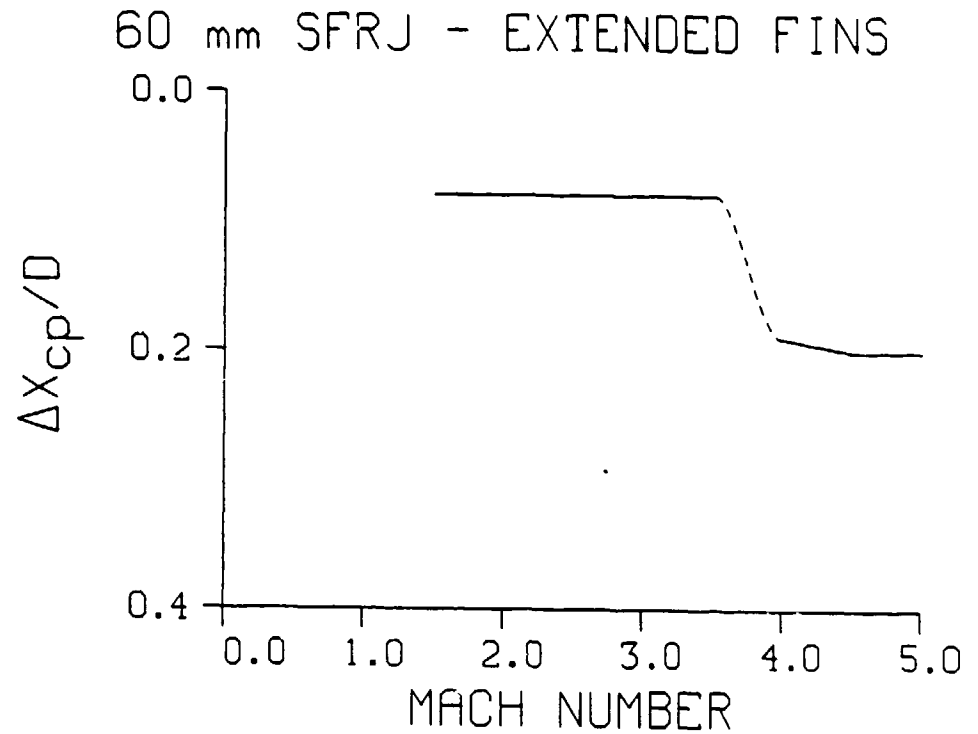

Figure 17. The effect of sting balance on the aerodynamic characteristics.
b. Center-of-pressure.

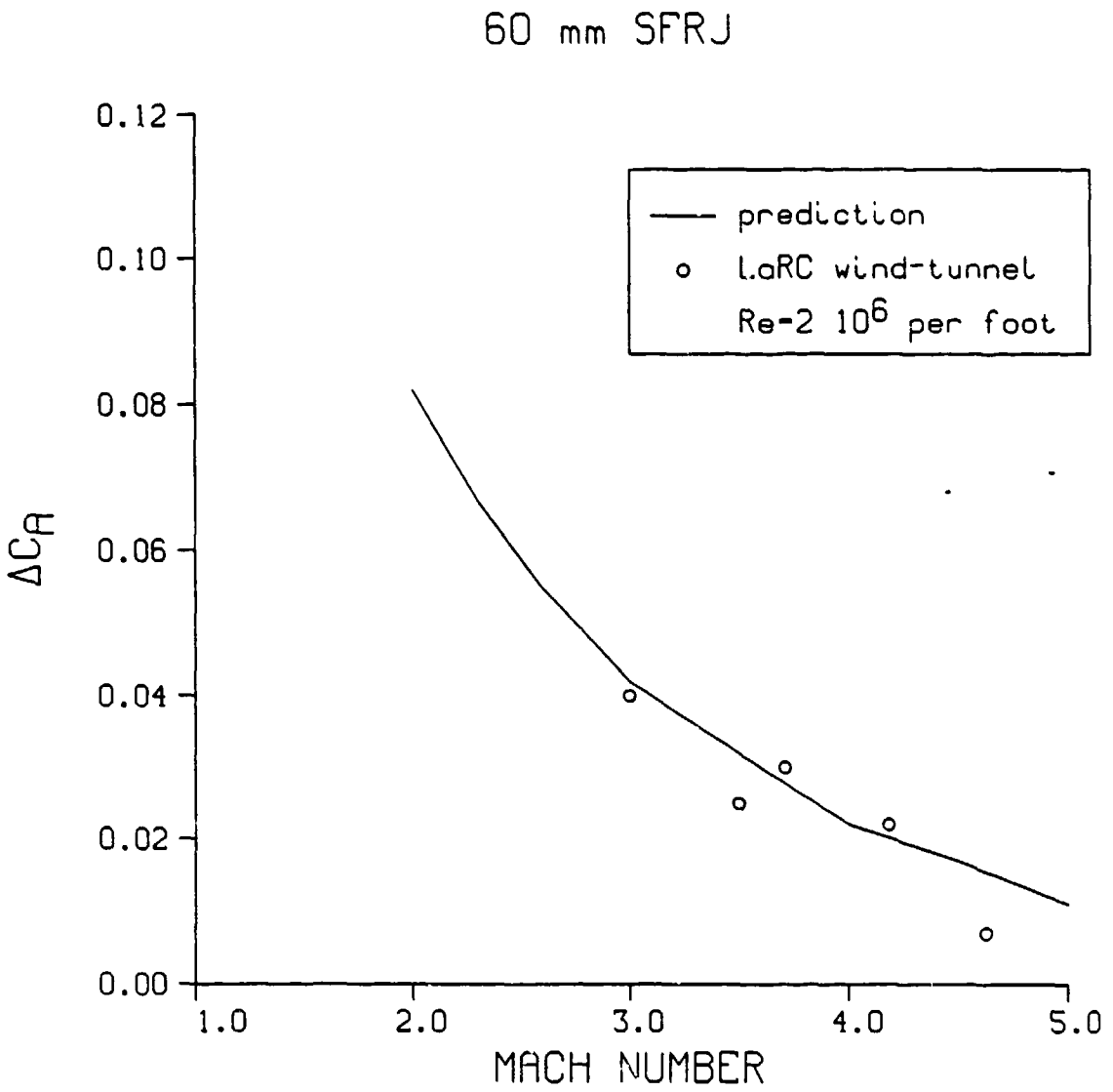

Figure 18. Comparison between predicted and experimentally obtained axial-force coefficient due to the buttress threads.

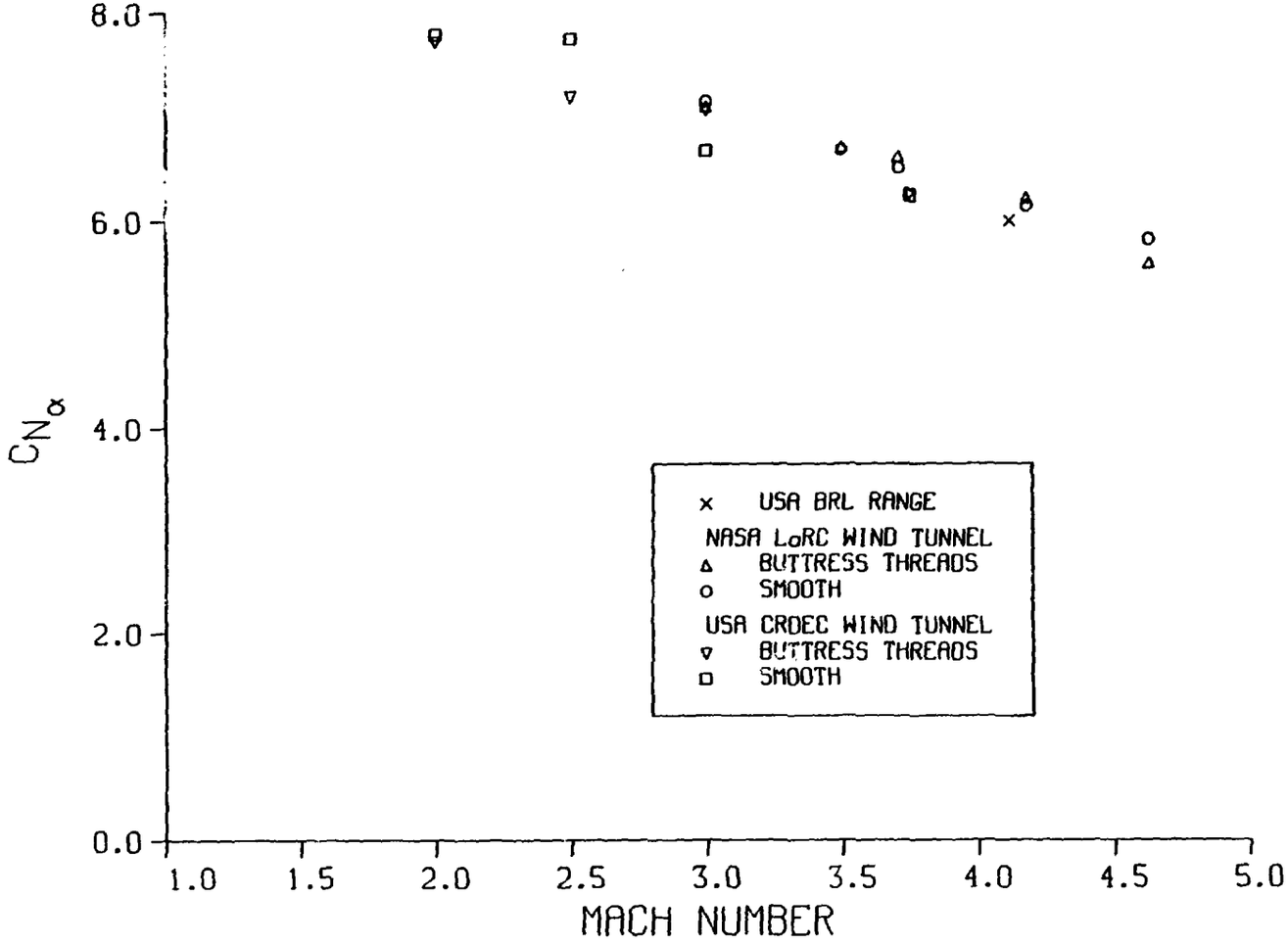

Figure 19. Experimentally obtained aerodynamic characteristics of the 60mm SFRJ projectile.

a. Normal-force curve slope.

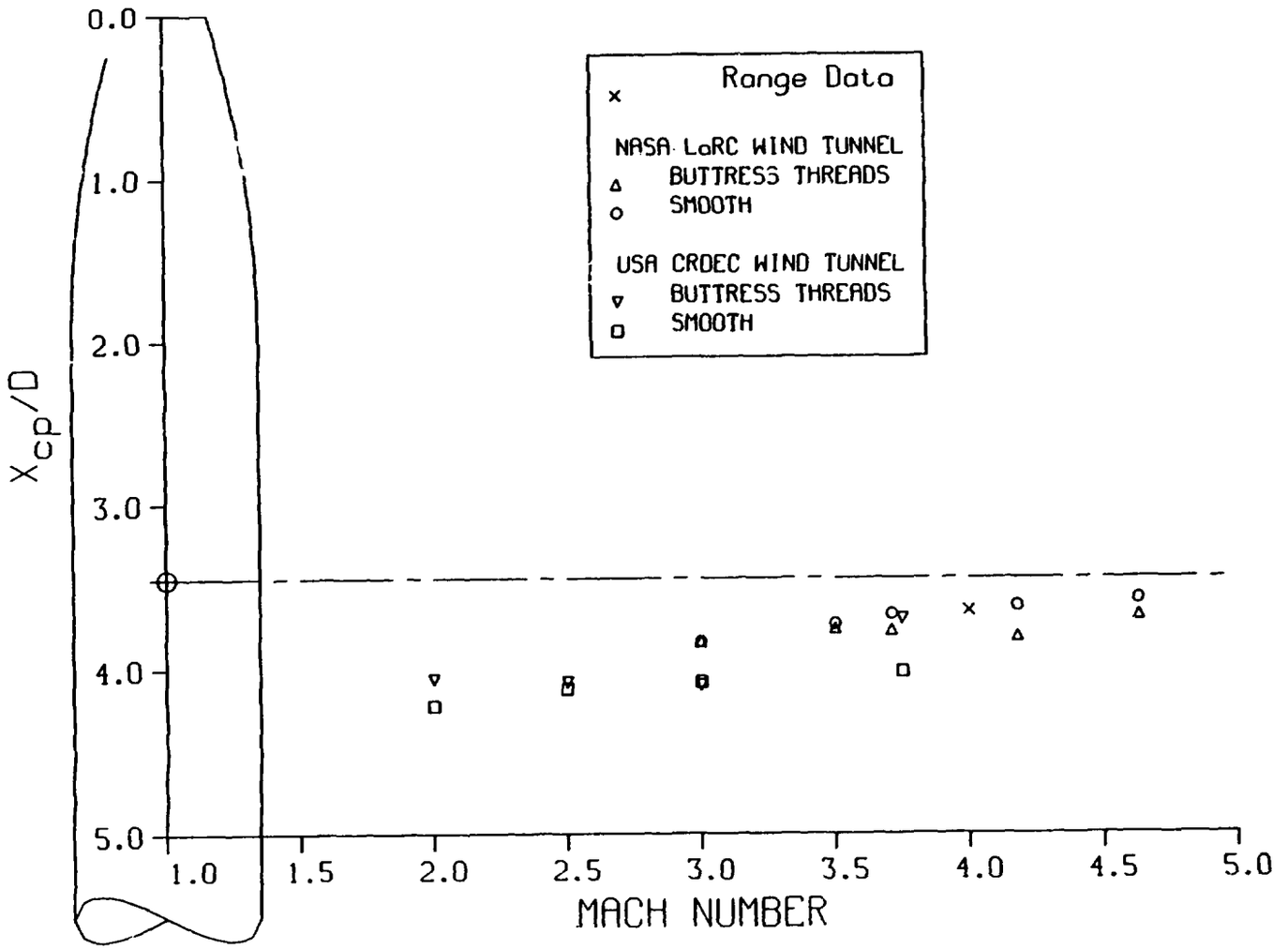

Figure 19. Experimentally obtained aerodynamic characteristics of the 60mm SFRJ projectile.

b. Center-of-pressure.

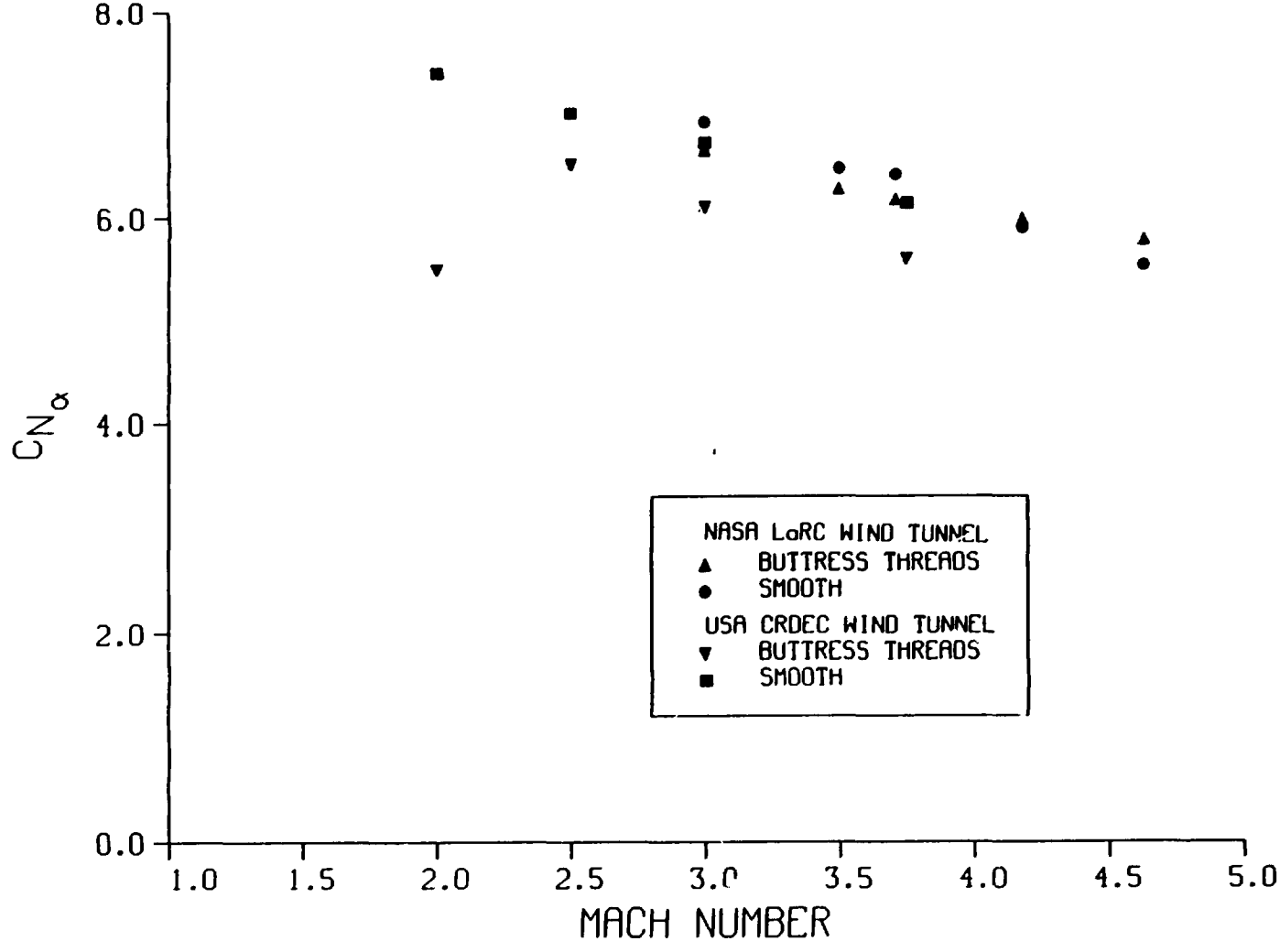

Figure 20. Experimentally obtained aerodynamic characteristics of the 60mm SFRJ projectile with extended nose.

a. Normal-force curve slope.

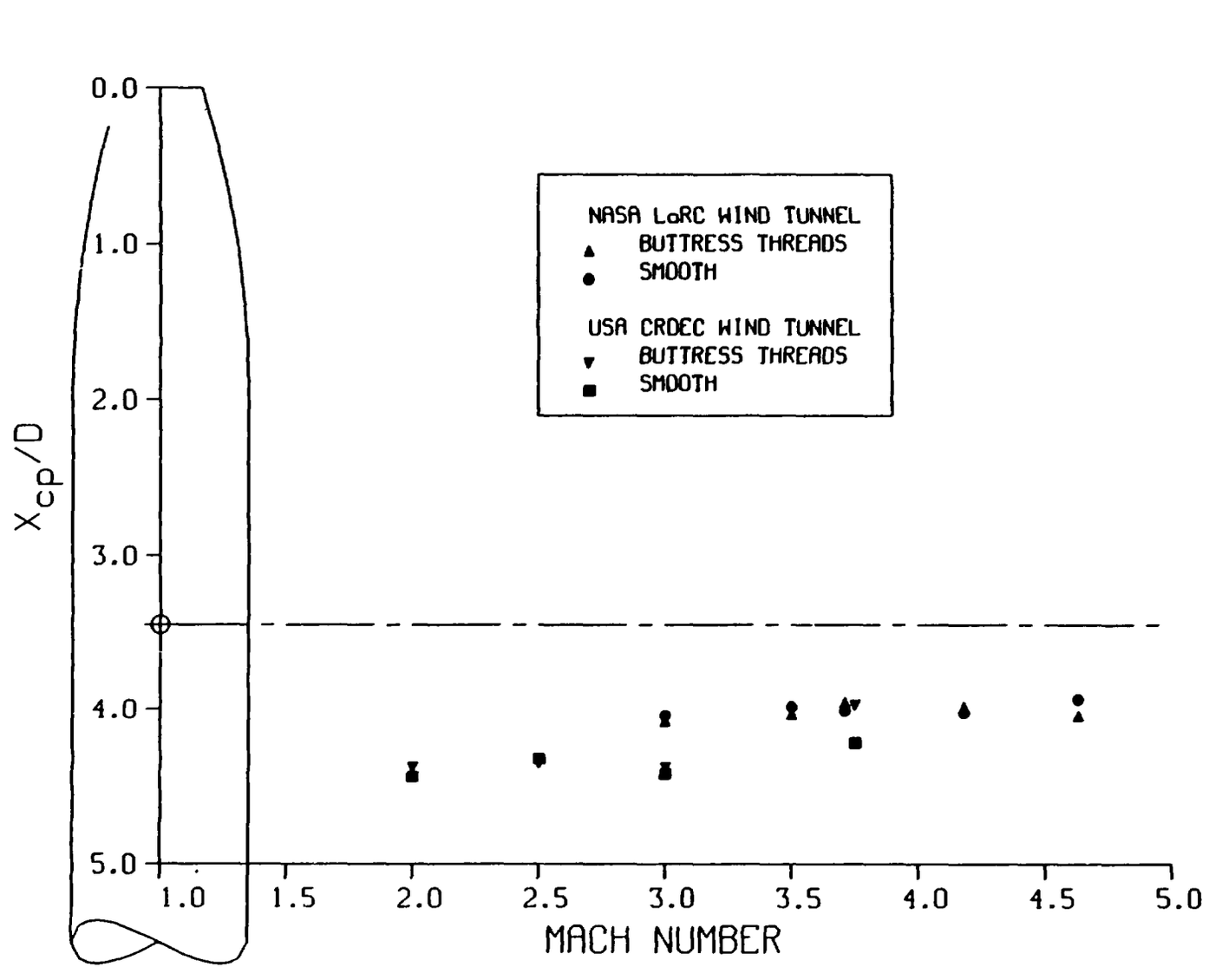

Figure 20. Experimentally obtained aerodynamic characteristics of the 60mm SFRJ projectile with extended nose.

b. Center-of-pressure.

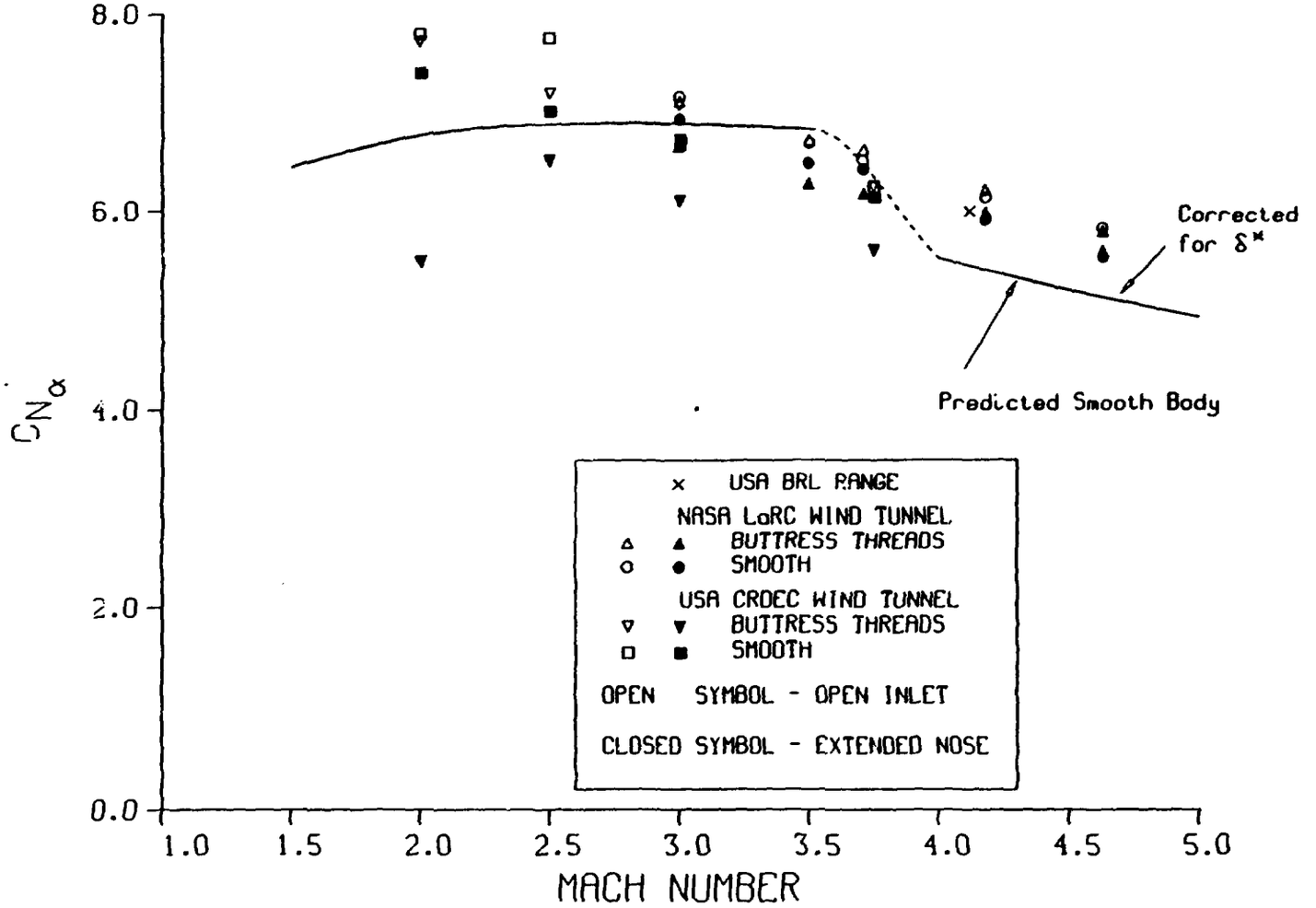

Figure 21. The effect of open inlet on the aerodynamic characteristics of the 60mm SFRJ projectile.

a. Normal-force curve slope.

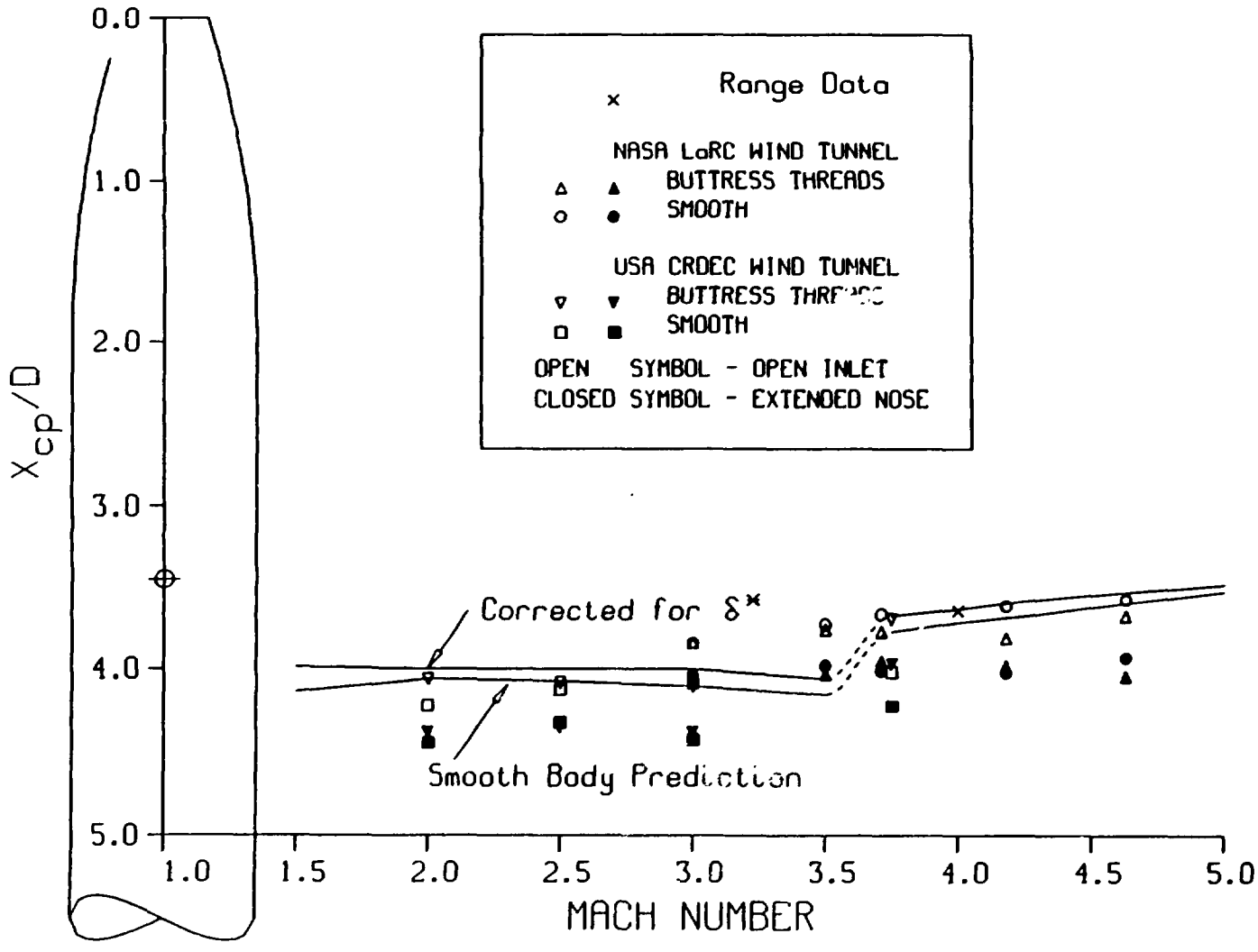

Figure 21. The effect of open inlet on the aerodynamic characteristics of the 60mm SFRJ projectile.

b. Center-of-pressure.

REFERENCES

1. Vukelich, S.R., Jenkins, J.E., "Missile DATCOM: Aerodynamic Prediction of Conventional Missiles Using Component Build-Up Techniques," AIAA Paper 84-0388, 1984

2 Mason, L.A., Devan, L., Moore, F.G., McMillan, D., "Aerodynamic Design Manual for Tactical Missiles," NSWC TR 81-156, 1981.

3. Van Dyke, M.D., "First- and Second-Order Theory of Supersonic Flow Past Bodies of Revolution," Journal of Aerospace Science, Vol. 18, No. 3, 1951.

4. Syvertson, C.A., Dennis, D.H., "A Second-Order Shock-Expansion Method Applicable to Bodies of Revolution Near Zero-Lift," NACA Report 1328, 1957.

5. Nielsen, J. "Missile Aerodynamics," McGraw-Hill Book Company LTD., 1960.

6. Stoney, A., "Collection of Zero-Lift Drag Data," NASA TR Report 100, 1962.

7. Hoerner, S., "Fluid Dynamic Drag," Published by the author, 1961.

8. Young, A.D., Paterson, J.H., "Aircraft Excrescence Drag," North Atlantic Treaty Organization, AGARD-AG-264, 1981.

9. Oskay, V., "Transonic Range Test of the 40mm SFRJ Projectile," BRL report in preparation, U.S. Army Ballistic Research Laboratory, Maryland.

10. Olson, D.N. and Wrede, F.G., "Wind Tunnel Test Results on a 34 Per Cent Scale Model of the Fin Stabilized Solid Fuel Ramjet Tubular Projectile at Mach Numbers of 2 to 3.75," CRDEC Technical Report to be published, Aberdeen Proving Ground, Maryland.

11. DATCOM-USAF Stability and Control Data Compendium, Second Edition, 1975.

12. Yalamanchili, R.J., "Transonic Range Test Results of the 75mm SFRJ Projectile," BRL report in preparation, US Army Ballistic Research Laboratory, Aberdeen Proving Ground, Maryland, 1986.

13. ESDU Data Units 5.01.03.01 and 5.08.03.01, Engineering and Scientific Data Units International, Ltd., 1983.

14. Fenter, F.W., "The Turbulent Boundary Layer on Uniformly Rough Surfaces at Supersonic Speeds," Chance Vought Research Center, Report No. RF-E9R-2, 1959.

15. Voisinet, R.L.P., "Influence of Roughness and Blowing on Compressible Turbulent Boundary Layer Flow," NSWC Dahalgren, Virginia, TR-79-153, 1979.

16. Shapiro, A., "The Aerodynamics and Thermodynamics of Compressible Fluid Flow," Vol. II, Chapter 27, The Ronald Press Company, 1954

17. Yalamanchili, R.J., Wood, R., Test results from NASA Unitary wind-tunnel on SFRJ to be published, Aberdeen Proving Ground, Maryland, October 1987.

18. Olson, D.N., Wrede, F., Test results from USA CRDEC supersonic wind-tunnel to be published, Aberdeen Proving Ground, Maryland, October 1987.

LIST OF SYMBOLS

AR	aspect ratio
B	$\sqrt{M^2 - 1}$
BT	buttress threads
c	chord
C_R	root chord
C_A	axial-force coefficient, based on reference area
C_{De}	drag coefficient of an excrescence, based on frontal area
C_N	normal-force coefficient
C_{N_α}	normal-force curve slope
C_M	pitching-moment coefficient
D	diameter of center body
D_i	diameter of inlet
h	height of a protuberance
H	boundary layer shape factor
$K_{T(B)}$	influence coefficient-tail in presence of body
$K_{B(T)}$	influence coefficient-body due to tail
l_e	length of extension of the nose
M	Mach number

S	area of exposed pair of fins
S_m	area masked by the boundary layer
S_R	reference area $\pi D^2/4$
X_{cp}	center-of-pressure measured from inlet lip

Greek Symbols

α	angle of attack
δ	boundary-layer thickness
δ^*	boundary-layer displacement thickness
δ^{**}	boundary-layer momentum thickness
η	tail efficiency factor

Subscripts

b	body
e	extended nose
f	fin assembly
i	inlet
o	open inlet
t	effective flare

Superscripts

s	series of protuberances
+	corrected
′	difference between open inlet and extended nose tip

DISTRIBUTION LIST

No. of Copies	Organization
12	Administrator Defense Technical Info Center ATTN: DTIC-FDAC Cameron Station, Bldg 5 Alexandria, VA 22304-6145
1	HQDA DAMA-ART-M Washington, DC 20310
1	Commander US Army Materiel Command ATTN: AMCDRA-ST 5001 Eisenhower Avenue Alexandria, VA 22333-0001
8	Commander US Army Armament Research, Development and Engineering Center ATTN: SMCAR-MSI SMCAR-LCA-F/Kline Fleming Kahn Hudgins SMCAR-CCL-CA/Hirlinger O'Niell Miller Dover, NJ 07801-5001
1	Commander US Army Armament Research, Development and Engineering Center ATTN: SMCAR-TDC Dover, NJ 07801-5001
1	Commander US AMCCOM ARDEC CCAC Benet Weapons Laboratory ATTN: SMCAR-CCB-TL Watervliet, NY 12189-4050
1	Commander US Army Armament, Munitions and Chemical Command ATTN: AMSMC-IMP-L Rock Island, IL 61299-7300
1	Commander US Army Aviation Systems Command ATTN: AMSAV-ES 4300 Goodfellow Blvd St. Louis, MO 63120-1798
1	Director US Army Aviation Research and Technology Activity Ames Research Center Moffett Field, CA 94035-1099
10	C.I.A. OIR/DB/Standard GE47 HQ Washington, DC 20505
1	Commander US Army Communications - Electronics Command ATTN: AMSEL-ED Fort Monmouth, NJ 07703-5301
1	Commander CECOM R&D Technical Library ATTN: AMSEL-IM-L (Reports Section) B.2700 Fort Monmouth, NJ 07703-5000
3	Commander US Army Missile Command Research, Development, and Engineering Center ATTN: AMSMI-RD Redstone Arsenal, AL 35898-5230
1	Director US Army Missile & Space Intelligence Center ATTN: AIAMS-YDL Redstone Arsenal, AL 35898-5500
1	Commander US Army Tank Automotive Command ATTN: AMSTA-TSL Warren, MI 48397-5000

DISTRIBUTION LIST

No. of Copies	Organization
1	Director US Army TRADOC Analysis Center ATTN: ATOR-TSL White Sands Missile Range, NM 88002-5502
2	Commander David W. Taylor Naval Ship ATTN: Dr. S. de los Santos Mr. Stanley Gottlieb Bethesda, MD 20084-5000
2	Commander US Naval Surface Weapons Center ATTN: Code DK20/Clare Moore Dahlgren, VA 22448-5000
1	Commandant US Army Infantry School ATTN: ATSH-CD-CS-OR Fort Benning, GA 31905-5400
1	Commander US Army Development and Employment Agency ATTN: MODE-ORO Fort Lewis, WA 98433-5000
1	AFWL/SUL Kirtland AFB, NM 87117
1	Air Force Armament Laboratory ATTN: AFATL/DLODL (Tech Info Ctr) Eglin AFB, FL 32542-5000
2	Sandia Laboratories ATTN: Dr. W.L. Oberkampf Dr. F. Blottner Division 1636 Albuquerque, NM 87185
1	Massachusetts Institute of Technology ATTN: Tech Library 77 Massachusetts Avenue Cambridge, MA 02139
4	Director NASA Ames Research Center ATTN: MS-202-1, Dr. T. Pulliam MS-258-1, Dr. J. Steger Dr. L. Schiff Moffett Field, CA 94035
1	Virginia Polytechnic Institute & State University P.O. Box 50 Blacksburg, VA 24061
1	University of Delaware Mechanical and Aerospace Engineering Department ATTN: K.L. Palko Newark, DE 19711
1	Commandant USAFAS ATTN: ATSF-TSM-CN Fort Sill, OK 73503-5600
2	Ford Aerospace and Communications Corporation Aeronutronic Division ATTN: Charles White Bud Blair Ford Road Newpoint Beach, CA 92658
2	Honeywell Inc. ATTN: Wilford E. Martwick Ken Sundeen 600 Second Street, North East Hopkins, MN 55343
1	NASA, Langley Research Center Transonic Aerodynamics Division ATTN: Dr. Michael J. Hemsch Hampton, VA 23665

DISTRIBUTION LIST

No. of Copies	Organization
	Aberdeen Proving Ground
	Dir, USAMSAA ATTN: AMXSY-D AMXSY-MP, H. Cohen
	Cdr, USATECOM ATTN: AMSTE-SI-F
	Cdr, CRDC, AMCCOM, ATTN: SMCCR-RSP-A SMCCR-MU SMCCR-SPS-IL

USER EVALUATION SHEET/CHANGE OF ADDRESS

This Laboratory undertakes a continuing effort to improve the quality of the reports it publishes. Your comments/answers to the items/questions below will aid us in our efforts.

1. BRL Report Number_____ Date of Report_____

2. Date Report Received_____

3. Does this report satisfy a need? (Comment on purpose, related project, or other area of interest for which the report will be used.)_____

4. How specifically, is the report being used? (Information source, design data, procedure, source of ideas, etc.)_____

5. Has the information in this report led to any quantitative savings as far as man-hours or dollars saved, operating costs avoided or efficiencies achieved, etc? If so, please elaborate._____

6. General Comments. What do you think should be changed to improve future reports? (Indicate changes to organization, technical content, format, etc.)

CURRENT ADDRESS

Name

Organization

Address

City, State, Zip

7. If indicating a Change of Address or Address Correction, please provide the New or Correct Address in Block 6 above and the Old or Incorrect address below.

OLD ADDRESS

Name

Organization

Address

City, State, Zip

(Remove this sheet, fold as indicated, staple or tape closed, and mail.)